A robust four-node quadrilateral element for laminated composite and sandwich plates based on Refined Zigzag Theory

A robust four-node quadrilateral element for laminated composite and sandwich plates based on Refined Zigzag Theory

M. Sorrenti[(1)*], M. Di Sciuva[(2)] and A. Tessler[(3)]

[(1)] Department of Mechanical and Aerospace Engineering – Politecnico di Torino, Corso Duca degli Abruzzi 24, 10129, Torino, Italy, matteo.sorrenti@polito.it

[(2)] Department of Mechanical and Aerospace Engineering – Politecnico di Torino, Corso Duca degli Abruzzi 24, 10129, Torino, Italy, marco.disciuva@polito.it

[(3)] Department of Mechanical and Aerospace Engineering – Politecnico di Torino, Corso Duca degli Abruzzi 24, 10129, Torino, Italy, alexander.tessler@polito.it and Structural Mechanics and Concepts Branch - NASA Langley Research Center, Mail Stop 190, Hampton, Virginia, 23681 - 2199, U.S.A., alexander.tessler-1@nasa.gov

Abstract

The paper presents a locking-free four-node element for laminated composite and sandwich plates based on Refined Zigzag Theory (RZT). Initially, two RZT-based plate elements are derived using four-node and eight-node configurations, achieved by way of standard C^0 isoparametric shape functions. In addition, with a view on improving the modelling of extremely thin plates, an anisoparametric four-node element is developed in which the transverse deflection variable is interpolated using quadratic polynomial shape functions, whereas the remaining kinematic variables are bilinear. A straightforward transverse-shear edge-constraint procedure gives rise to a four-node anisoparametric element. A further enhancement is achieved using an Element Shear Correction (ESC) factor that is derived from a strain-energy matching procedure. The resulting four-node element (ZQ4c) uses full Gauss quadrature, consistent load vector, and mass matrix. Furthermore, the ZQ4c stiffness matrix has no spurious zero-energy modes, and the element is extremely robust when modelling ultra-thin plates. Several numerical studies are carried out to demonstrate the predictive capabilities of the four elements examined in this investigation. It is concluded ZQ4c is a highly accurate element over a wide range of material systems and span-to-thickness ratios, and is the best performing element of the four elements examined in this study.

https://doi.org/10.1016/j.compstruc.2020.106369

Keywords: Refined Zigzag Theory; Quadrilateral plate element; Transverse shear locking; Anisoparametric interpolation; Multi-layered composite and sandwich plates

* Corresponding Author: Matteo Sorrenti, email: matteo.sorrenti@polito.it Tel. +39 3337120343.

1. Introduction

Multi-layered composite and sandwich structures, used extensively in civil, defense, marine and aerospace structures, require accurate models to describe the structural behaviour. Due to the complex nature of anisotropic and heterogeneous material systems, the analytical models require inclusion of transverse-shear deformability in order to achieve relatively accurate predictions of their structural response. In the framework of the displacement-based theories, three general approaches are commonly used [1,2]: the Equivalent Single Layer theories (ESL), the Layer-Wise (LW) theories and the Zigzag (ZZ) theories. In the ESL theories, a smoothly continuous through-the-thickness distribution of the displacement field is assumed across the entire laminate thickness; with these assumptions resulting in discontinuities of the transverse stresses along layer interfaces. Among these theories, Classical Plate Theory (CPT), First-order Shear Deformation Theory (FSDT) and Third-order Shear Deformation Theory (TSDT) are commonly used [1,2]. For thin plates, CPT is generally accurate to predict such global response quantities as deflections, buckling loads, and lower vibrational frequencies and their mode shapes. FSDT is the simplest shear-deformation theory using the concept of independent bending-rotation variables. For multi-layered composite plates, the theory gives rise to thickness-wise constant distributions of the transverse-shear strains, and piecewise-constant transverse-shear stresses, thus requiring the use of appropriate shear correction factors [3,4].

To achieve more accurate predictions, Higher-order Shear Deformation theories (HSDT, [5–7]), of which TSDT is a special case, have been developed. Many of these theories generally provide improved global response predictions without the use of shear correction factors. As in FSDT, however, the interface transverse stresses cannot achieve continuity using such theories. Finite elements derived on the basis of such theories require C^1 continuity for the transverse displacement whereas FSDT requires only C^0 continuity.

In LW theories, each layer has its own independent displacement field, which leads to a quasi-3D description of the structure. This aspect assures a high degree of accuracy, but for laminates with many layers in complex structures, the computational cost is prohibitively high; for further details the reader is referred to the review article of Liew et al. [8]. A reasonable compromise between the computationally efficient FSDT and the highly accurate LW theories is represented by the zigzag theories (ZZ). In ZZ theories, the displacement kinematic field is assumed as a superposition of the global laminate behaviour and a local (layer scale) kinematic refinement. This improved kinematic description generally results in predicting more accurate piecewise behaviour through the laminate thickness, resembling those of three-dimensional (3D) elasticity solutions. Similar to ESL theories, zigzag theories have a fixed number of kinematic variables and they are independent on the number of material layers in a laminate. Generally, zigzag theories provide accurate response

predictions for relatively thick laminated-composite and sandwich structures, comparable in accuracy to LW theories. In the pioneering zigzag theories of Di Sciuva, the kinematics of FSDT are augmented using piecewise linear [9–11] and cubic [12,13] functions. Using a similar concept, Murakami [14] proposed zigzag functions for periodic laminated structures; Icardi [15,16] developed a 3D zigzag theory for the analysis of composite beams. Averill developed linear [17] and cubic [18] zigzag beam models from Timoshenko-beam assumptions.

Recently, Tessler and co-workers proposed the Refined Zigzag Theory (RZT) for beams [19], plates [20] and shells [21]. The relative accuracy and performances of RZT have been extensively investigated. The interested reader is referred to this non-exhaustive list: Tessler et al [22] investigated the use of homogeneous material and RZT; the effect of external weak layers was assessed by Gherlone [23]; Iurlaro et al [24] assessed RZT for the static, dynamic and stability analysis of multi-layered composites and sandwich structures; Iurlaro et al [25] and Di Sciuva et al [26,27] performed RZT analysis of functionally graded plates; Groh et al [28,29] applied RZT to modelling and studying highly heterogeneous and delaminated beams; Dorduncu [30] used RZT in combination with the peridynamic operator to study heterogeneous beams. A recent application of RZT is represented by work of Tessler [31] in which it combined the kinematic assumption of RZT and the Reissner's Mixed Variational Theorem (RMTV) to satisfy a priori the transverse shear stress continuity. This new approach named RZT$^{(m)}$ has been used by Groh et al [32] for beam and by Iurlaro et al [33] for plates analysis.

Similar to FSDT, RZT is computationally attractive because (1) the theory has a small, fixed number of kinematic variables regardless of the number of material layers, and (2) its kinematic finite element approximations need not exceed C^0 continuity. Thus, using RZT as a theoretical basis, various computationally efficient and highly accurate finite elements have been developed for beam [32,34–37], plate [38–42] and shell [21,43] analyses.

One detrimental effect commonly associated with C^0-continuous shear-deformable finite elements is known as *shear locking* – an overly stiff response prediction of thin-to-ultra thin structures undergoing bending deformations. This phenomenon has been widely investigated using low-order isoparametric approximations of Timoshenko beam and Mindlin plate finite elements, i.e., elements derived from a class of FSDT. The shear locking effect can also detrimentally affect RZT-based finite elements based on low-order isoparametric interpolations even for moderately thin beams and plates [35,38,41]. In the open literature, different approaches have been explored to remedy the shear locking effect. The most widely used technique is called *reduced* integration. Essentially, the transverse shear strain energy is "under integrated" [44] using a lower-order Gauss quadrature formula. Even though *reduced integration* can often overcome *shear locking*, the element generally requires ad hoc stabilization techniques to suppress undesirable spurious energy modes [45–48]. Other strategies adopted to overcome the transverse shear locking problem have been exposed in details

in Ref. [41]. For the Timoshenko beam element, Tessler and Dong [49] identified the reason for *shear-locking* effect in the Kirchhoff constraints of the shear strain measure for very thin structures. As a possible solution, they proposed to use the *anisoparametric* interpolation, where the transverse deflection is approximated by a polynomial with one order degree higher than the others used for the remaining kinematic variable (bending rotations). These elements, named *unconstrained anisoparametric elements* by Tessler and Dong [49], have one extra node in the middle beam point having only the transverse degree of freedom (dof). The same strategy has been implemented by Tessler and Hughes [50,51] for quadrilateral and triangular Mindlin plate elements. To achieve the simplest configuration (two-node for beam element, three-node for triangular plate element or four-node for quadrilateral plate element), the *edge-constrained* strategy is adopted, in which the mid-side dof's (transverse displacement dof) are made dependent of the vertex dof's. This strategy was successfully implemented to the formulation of beam [49,52], plate [50,51] and shell [53,54] elements. Gherlone et al [34] and Di Sciuva et al [37] formulated RZT beam elements in conjunction with the *constrained anisoparametric strategy*. Moreover, Versino et al [40] applied this strategy to the triangular plate elements and Gherlone [42] to three and four-node elements based on $RZT^{(m)}$. Recently Di Sciuva and Sorrenti [41] compared the linear four-node, the serendipity eight-node and the four-node *constrained* element based on RZT, showing that the *constrained anisoparametric* technique alleviates the shear locking problem up to thin plates (span-to-thickness ratio $a/h=10^3$) without solving it. To avoid the shear-locking problem definitively, Tessler and Hughes [50,51] introduced a new finite element appropriate shear correction factor to use in combination with the shear correction factor used for Mindlin theory. Using the deflection matching technique [50] or the minimization of the total potential energy method [51], for FSDT it has been possible to obtain well-conditioned element stiffness matrix for over the entire range of the thickness-to-length ratios, guaranteeing rapid convergence solutions.

The purpose of this work is to provide robust four-node finite element based on RZT, derived from the *constrained anisoparametric* strategy, capable to describe the behaviour of sandwich and multi-layered composite structures with good accuracy and reliability for various thickness-to-length ratios without incurring the problem of shear locking.

The present work is organized as follow.

In Section 2, the kinematic assumptions of RZT are presented, and the discretized equations of motion are obtained for laminated composite and sandwich plates using the dynamics principle of virtual work. In Section 3, the RZT finite element formulations are discussed, together with a derivation of the element shear correction factor. In Section 4, numerical studies are performed to critically examine the predictive capabilities of the new RZT elements over a wide range of thickness-to-span plate ratios. Finally, in Section 5, conclusions are presented highlighting the main findings of this research.

2. Theoretical basis of Refined Zigzag Theory for plate

In this Section, the kinematic assumptions of RZT are presented, and the discretized equations of motion are obtained for laminated composite and sandwich plates using the dynamics principle of virtual work.

2.1 Displacement and zigzag kinematic

We consider a multilayered flat plate made of a finite number N_L of perfectly bonded layers. V is the volume of the plate, h the thickness. The thickness of each layer, as well as of the whole plate, is assumed to be constant, and the material of each layer is assumed to be linearly elastic and orthotropic with a plane of elastic symmetry parallel to the reference surface and whose principal orthotropy directions are arbitrarily oriented with respect to the reference frame. The points of the plate are referred to an orthogonal Cartesian coordinate system $\mathbf{X} = \{x_j\}$ $(j = 1,2,3)$, where $\mathbf{x} = \{x_\alpha\}$ $(\alpha = 1,2)$ is the set of in-plane coordinates on the reference plane, here chosen to be the middle plane of the plate, and $x_3 \equiv z$ is the co-ordinate normal to the reference plane (Fig. 1); the origin of the reference frame is fixed at the middle plane of the plate, so that, x_3 is defined in the range $x_3 \in \left[-\frac{h}{2}, +\frac{h}{2}\right]$. We denote with Ω_m the set of points of the middle-plane of the plate. The intersection between the middle-plane and the lateral surface of the plate gives the total perimeter, Γ, surrounding the region Ω_m.

If not otherwise stated, in the paper the superscript (k) is used to indicate quantities corresponding to the kth layer (k=1,N_L), whereas the subscript (k) defines quantities corresponding to the kth interface (k=1,N_L-1) between the k and (k+*1*) layer. So, in the following, the symbol $(.)_{(k)}$ stands for (.) valued at $x_3 = z_{(k)}$, i.e., at the k-th interface. Also, we use the subscript b and t to indicate the top and bottom surfaces of the plate; specifically, $z_{(0)} = z_b$ and $z_{(N_L)} = z_t$ denote the coordinates of the bottom and top surfaces of the whole plate; thus, $h = z_t - z_b$ is the plate thickness and $h^{(k)} = z_{(k)} - z_{(k-1)}$ $(k = 1,2,...,N_L)$, the thickness of the kth layer (see Figure 1).

The plate is subjected to a transverse load $\bar{q}_z$ applied on the midplane surface of the plate (Ω_m) and defined as positive in the positive z direction and boundary transverse load per unit-length $(\bar{F}_z)$applied along the perimeter of the plate (Γ) (see, Figure 1). The symbol $(\bullet)_{,i} = \frac{\partial(\bullet)}{\partial x_i}$ refers to the derivative of the function $(\bullet)$ with respect to the coordinate x_i, i.e., $(\bullet)_{,i} = \frac{\partial(\bullet)}{\partial x_i}$. In the paper, if not otherwise specified, the Einsteinian summation convention over repeated indices is adopted, with Latin indices ranging from 1 to 3, and Greek indices ranging from 1 to 2.

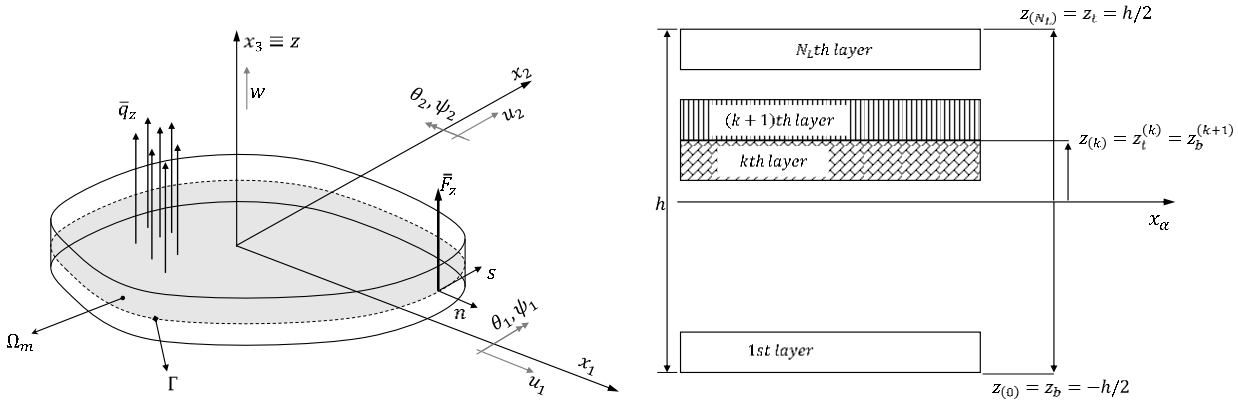

Figure 1 - Plate and layers notation, geometry and coordinate system.

As usual in the axiomatic approach of theories of plate and shells, the law of variation of the 3-D displacement field at time *t* for a point within the *k*th layer is a-priori assumed along the thickness. Thus, in general we can write

$$\mathbf{u}^{(k)}(x_j,t) = \mathbf{Z}^{(k)}(z)\mathbf{d}(x_\alpha,t) \tag{1}$$

where

$$\mathbf{u}^{(k)}(x_j,t) = \begin{Bmatrix} \tilde{u}_1(x_j,t) \\ \tilde{u}_2(x_j,t) \\ \tilde{u}_3(x_j,t) \end{Bmatrix} = \begin{Bmatrix} \tilde{\mathbf{u}}(x_j,t) \\ w(x_j,t) \end{Bmatrix} \tag{2}$$

is the vector of displacement components of the generic point belonging to the *k*th layer; $\mathbf{d}(x_\alpha,t)$ is the vector of the generalized displacements, independent of the *z*-coordinate, and $\mathbf{Z}^{(k)}(z)$ is the matrix of the assumed thickness-wise distributions. Both $\mathbf{d}(x_\alpha,t)$ and $\mathbf{Z}^{(k)}(z)$ are plate/shell theory dependent. With reference to RZT (see, Refs. [20,22,55]), the transverse displacement is assumed to be constant through-the-thickness, i.e.

$$\tilde{u}_3(x_j,t) = u_3(x_\alpha,t) = w(x_\alpha,t) \tag{3}$$

The in-plane kinematic is based on the superposition of a global (G) first-order kinematic (from FSDT plate theory) and a local (L) layer-wise correction of the in-plane displacements (continuous with respect to *z*, but with jumps in the first derivative at the interface between adjacent layers), (see, Fig. 2). Thus,

$$\tilde{\mathbf{u}}(x_j,t) = \begin{Bmatrix} \tilde{u}_1(x_j,t) \\ \tilde{u}_2(x_j,t) \end{Bmatrix} = \begin{Bmatrix} \tilde{u}_1^G(x_j,t) \\ \tilde{u}_2^G(x_j,t) \end{Bmatrix} + \begin{Bmatrix} \tilde{u}_1^L(x_j,t) \\ \tilde{u}_2^L(x_j,t) \end{Bmatrix} = \begin{Bmatrix} u_1(x_\alpha,t) + z\theta_1(x_\alpha,t) \\ u_2(x_\alpha,t) + z\theta_2(x_\alpha,t) \end{Bmatrix} + \begin{Bmatrix} \phi_1^{(k)}(z)\psi_1(x_\alpha,t) \\ \phi_2^{(k)}(z)\psi_2(x_\alpha,t) \end{Bmatrix} \tag{4}$$

In Eq. (4), u_1 and u_2 are the uniform displacements along the x_1- and x_2- axis (coincident with those of a point belonging to the middle plane of the plate, for symmetric laminate); θ_1 and θ_2 are the bending rotations of the normal to

the middle surface along with the directions $+x_2$ and $-x_1$, respectively, and *w* is the transverse deflection, assumed to be constant along the thickness. ψ_1 and ψ_2 represent the spatial amplitudes of the zigzag functions $\phi_1^{(k)}$ and $\phi_2^{(k)}$, respectively (see Figure 1). It can be easily found that FSDT is a special case of RZT, i.e. when in Eq.(4) $\tilde{u}_\alpha^{L(k)} = 0 \quad (\alpha = 1,2)$.

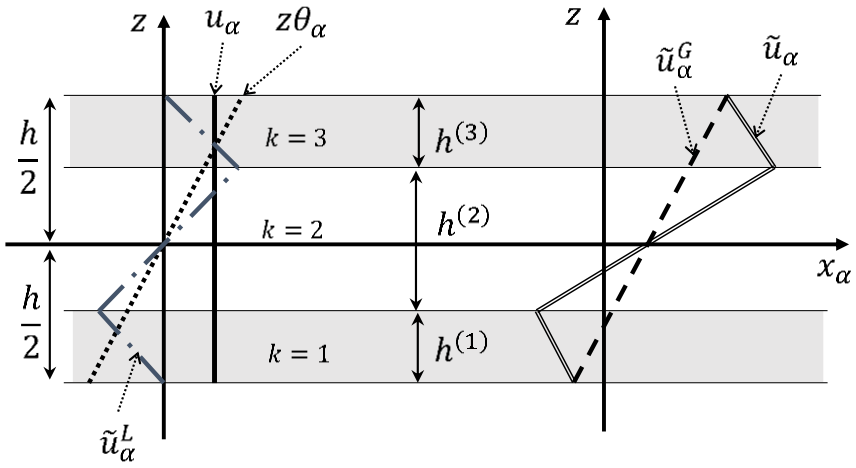

Figure 2 - Contributions to the in-plane RZT kinematic for a three-layered laminate.

Substituting Eqs. (3)-(4) in Eq. (1), gives

$$\mathbf{d}^T = \lfloor u_1 \quad u_2 \quad u_3 \quad \theta_1 \quad \theta_2 \quad \psi_1 \quad \psi_2 \rfloor \tag{5}$$

$$\mathbf{Z}^{(k)} = \begin{bmatrix} 1 & 0 & 0 & z & 0 & \phi_1^{(k)}(z) & 0 \\ 0 & 1 & 0 & 0 & z & 0 & \phi_2^{(k)}(z) \\ 0 & 0 & 1 & 0 & 0 & 0 & 0 \end{bmatrix} = \begin{bmatrix} \mathbf{I} & \mathbf{0} & z\mathbf{I} & \boldsymbol{\phi}^{(k)} \\ \mathbf{0} & 1 & \mathbf{0} & \mathbf{0} \end{bmatrix} \tag{6}$$

For the *k*th layer of thickness $h^{(k)}$, the refined zigzag functions have the following expressions [55]:

$$\begin{aligned}
&\phi_1^{(1)}(z) = (z + \frac{h}{2})\left(\frac{G_4}{\bar{Q}_{44}^{(1)}} - 1\right) && (k = 1) \\
&\phi_2^{(1)}(z) = (z + \frac{h}{2})\left(\frac{G_5}{\bar{Q}_{55}^{(1)}} - 1\right) && (k = 1) \\
&\phi_1^{(k)}(z) = (z + \frac{h}{2})\left(\frac{G_4}{\bar{Q}_{44}^{(k)}} - 1\right) + \sum_{q=2}^{k} h^{(q-1)}\left(\frac{G_4}{\bar{Q}_{44}^{(q-1)}} - \frac{G_4}{\bar{Q}_{44}^{(k)}}\right) && (k = 2,...,N_L) \\
&\phi_2^{(k)}(z) = (z + \frac{h}{2})\left(\frac{G_5}{\bar{Q}_{55}^{(k)}} - 1\right) + \sum_{q=2}^{k} h^{(q-1)}\left(\frac{G_5}{\bar{Q}_{55}^{(q-1)}} - \frac{G_5}{\bar{Q}_{55}^{(k)}}\right) && (k = 2,...,N_L)
\end{aligned} \tag{7}$$

where

$$G_j = \left(\frac{1}{h}\sum_{k=1}^{N_L}\int_{z_b^{(k)}}^{z_t^{(k)}} \frac{dz}{\bar{Q}_{jj}^{(k)}}\right)^{-1} \quad (j = 4,5) \tag{8}$$

and $\bar{Q}_{jj}^{(k)}$ is the transformed reduced transverse shear stiffness modulus of the *k*th layer (see, Eq. (16)).

Eqs. (7) and (8) show that the *refined zigzag functions* $\phi_\alpha^{(k)}$ are *a-priori* known piecewise continuous functions of *z*, depend only on the thickness and transverse shear mechanical properties of the constituent layers and vanish on the bottom $\left(z=-\frac{h}{2}\right)$ and top $\left(z=+\frac{h}{2}\right)$ surfaces of the plate (see, Figure 2).

In Eq. (6) and in the body of the paper, **I** stands for the identity matrix and **0** for the null rectangular matrix, which dimensions follow from the rule of the matrix product and partitioning.

2.2 Strains, stresses and constitutive relations

From the displacement field expressed by Eqs. (1), the linear strain expressions for the *kth* layer can be obtained from the relationships

$$\tilde{\boldsymbol{\varepsilon}}^{(k)}=\begin{Bmatrix}\tilde{u}_{1,1}\\ \tilde{u}_{2,2}\\ \tilde{u}_{1,2}+\tilde{u}_{2,1}\\ \tilde{u}_{1,3}+\tilde{u}_{3,1}\\ \tilde{u}_{2,3}+\tilde{u}_{3,2}\end{Bmatrix}=\begin{Bmatrix}\tilde{\boldsymbol{\varepsilon}}_p^{(k)}\\ \tilde{\boldsymbol{\gamma}}^{(k)}\end{Bmatrix},\quad \tilde{\boldsymbol{\varepsilon}}_p^{(k)}=\begin{Bmatrix}\tilde{\varepsilon}_{11}\\ \tilde{\varepsilon}_{22}\\ \tilde{\gamma}_{12}\end{Bmatrix}^{(k)}=\begin{Bmatrix}\tilde{u}_{1,1}\\ \tilde{u}_{2,2}\\ \tilde{u}_{1,2}+\tilde{u}_{2,1}\end{Bmatrix}^{(k)},\quad \tilde{\boldsymbol{\gamma}}^{(k)}=\begin{Bmatrix}\tilde{\gamma}_{13}\\ \tilde{\gamma}_{23}\end{Bmatrix}^{(k)}=\begin{Bmatrix}\tilde{u}_{1,3}+w_{,1}\\ \tilde{u}_{2,3}+w_{,2}\end{Bmatrix}^{(k)} \tag{9}$$

These can be written in compact form as

$$\tilde{\boldsymbol{\varepsilon}}^{(k)}=\mathbf{Z}_\varepsilon\boldsymbol{\varepsilon}=\mathbf{Z}_\varepsilon\left(\nabla_\varepsilon\mathbf{d}\right) \tag{10}$$

where

$$\boldsymbol{\varepsilon}=\begin{Bmatrix}\boldsymbol{\varepsilon}_m\\ \boldsymbol{\varepsilon}_b\\ \boldsymbol{\varepsilon}_\psi\\ \boldsymbol{\gamma}^{(0)}\\ \boldsymbol{\psi}\end{Bmatrix},\quad \boldsymbol{\varepsilon}_m=\begin{Bmatrix}u_{1,1}\\ u_{2,2}\\ u_{1,2}+u_{2,1}\end{Bmatrix},\quad \boldsymbol{\varepsilon}_b=\begin{Bmatrix}\theta_{1,1}\\ \theta_{2,2}\\ \theta_{1,2}+\theta_{2,1}\end{Bmatrix},\quad \boldsymbol{\varepsilon}_\psi=\begin{Bmatrix}\psi_{1,1}\\ \psi_{2,2}\\ \psi_{1,2}\\ \psi_{2,1}\end{Bmatrix},\quad \boldsymbol{\gamma}^{(0)}=\begin{Bmatrix}\theta_1+w_{,1}\\ \theta_2+w_{,2}\end{Bmatrix} \tag{11}$$

$$\mathbf{Z}_\varepsilon=\begin{bmatrix}\mathbf{I} & z\mathbf{I} & \boldsymbol{\Phi}^{(k)} & \mathbf{0} & \mathbf{0}\\ \mathbf{0} & \mathbf{0} & \mathbf{0} & \mathbf{I} & \boldsymbol{\beta}^{(k)}\end{bmatrix},\quad \boldsymbol{\Phi}^{(k)}=\begin{bmatrix}\phi_1^{(k)} & 0 & 0 & 0\\ 0 & \phi_2^{(k)} & 0 & 0\\ 0 & 0 & \phi_1^{(k)} & \phi_2^{(k)}\end{bmatrix},\quad \boldsymbol{\beta}^{(k)}=\begin{bmatrix}\beta_1^{(k)} & 0\\ 0 & \beta_2^{(k)}\end{bmatrix} \tag{12}$$

where $\beta_\alpha^{(k)}=\phi_{\alpha,z}^{(k)}\ \ (\alpha=1,2)$.

$$\nabla_{\varepsilon}^{T}=\begin{bmatrix}(\bullet)_{,x_1} & 0 & (\bullet)_{,x_2} & 0 & 0 & 0 & 0 & 0 & 0 & 0 & 0 & 0 & 0 & 0\\ 0 & (\bullet)_{,x_2} & (\bullet)_{,x_1} & 0 & 0 & 0 & 0 & 0 & 0 & 0 & 0 & 0 & 0 & 0\\ 0 & 0 & 0 & 0 & 0 & 0 & 0 & 0 & 0 & 0 & (\bullet)_{,x_1} & (\bullet)_{,x_2} & 0 & 0\\ 0 & 0 & 0 & (\bullet)_{,x_1} & 0 & (\bullet)_{,x_2} & 0 & 0 & 0 & 0 & 1 & 0 & 0 & 0\\ 0 & 0 & 0 & 0 & (\bullet)_{,x_2} & (\bullet)_{,x_1} & 0 & 0 & 0 & 0 & 0 & 1 & 0 & 0\\ 0 & 0 & 0 & 0 & 0 & 0 & (\bullet)_{,x_1} & 0 & (\bullet)_{,x_2} & 0 & 0 & 0 & 1 & 0\\ 0 & 0 & 0 & 0 & 0 & 0 & 0 & (\bullet)_{,x_2} & 0 & (\bullet)_{,x_1} & 0 & 0 & 0 & 1\end{bmatrix} \tag{13}$$

By taking into account the assumed displacement field, Eq. (1), and assuming, as usual in plate theory, $\tilde{\sigma}_{33}=0$, yields

$$\tilde{\boldsymbol{\sigma}}^{(k)}=\begin{Bmatrix}\tilde{\boldsymbol{\sigma}}_p^{(k)}\\ \tilde{\boldsymbol{\sigma}}_t^{(k)}\end{Bmatrix},\quad \tilde{\boldsymbol{\sigma}}_p^{(k)}=\begin{Bmatrix}\tilde{\sigma}_{11}\\ \tilde{\sigma}_{22}\\ \tilde{\sigma}_{12}\end{Bmatrix}^{(k)},\quad \tilde{\boldsymbol{\sigma}}_t^{(k)}=\begin{Bmatrix}\tilde{\sigma}_{13}\\ \tilde{\sigma}_{23}\end{Bmatrix}^{(k)} \tag{14}$$

The constitutive equations for a generally orthotropic layer are

$$\tilde{\boldsymbol{\sigma}}^{(k)}=\bar{\mathbf{Q}}^{(k)}\tilde{\boldsymbol{\varepsilon}}^{(k)} \tag{15}$$

where

$$\bar{\mathbf{Q}}^{(k)}=\begin{bmatrix}\bar{\mathbf{Q}}_p^{(k)} & \mathbf{0}\\ \mathbf{0} & \bar{\mathbf{Q}}_t^{(k)}\end{bmatrix},\quad \bar{\mathbf{Q}}_p^{(k)}=\begin{bmatrix}\bar{Q}_{11} & \bar{Q}_{12} & \bar{Q}_{16}\\ \bar{Q}_{12} & \bar{Q}_{22} & \bar{Q}_{26}\\ \bar{Q}_{16} & \bar{Q}_{26} & \bar{Q}_{66}\end{bmatrix}^{(k)},\quad \bar{\mathbf{Q}}_t^{(k)}=\begin{bmatrix}\bar{Q}_{44} & \bar{Q}_{45}\\ \bar{Q}_{45} & \bar{Q}_{55}\end{bmatrix}^{(k)} \tag{16}$$

and $\bar{Q}_{ij}^{(k)}$ (i,j=1,2,6) and and $\bar{Q}_{ij}^{(k)}$ (*i*,*j*=4,5) are the plane stress transformed stiffness moduli of the *k*th layer, that are functions of the z-coordinate. Typically, for orthotropic materials, $\bar{Q}_{45}^{(k)}=0$.

2.3 Principle of Virtual Work and equations of motion

The discretized equations of motion are obtained using the dynamics principle of virtual work, also known as D'Alembert's principle

$$\delta U-\delta W_{ext}=\delta W_{in} \tag{17}$$

where δ is the variational operator, δU is the virtual work done by the internal forces (stresses); δW_{in} is the virtual work done by the inertial forces, and δW_{ext} is the virtual work done by the applied forces.

The virtual work done by the internal stresses can be expressed as

$$\boldsymbol{\delta U}=\int_{\Omega_m}\left\langle\delta\tilde{\boldsymbol{\varepsilon}}_p^{(k)T}\tilde{\boldsymbol{\sigma}}_p^{(k)}+\delta\tilde{\boldsymbol{\gamma}}^{(k)T}\tilde{\boldsymbol{\sigma}}_t^{(k)}\right\rangle d\Omega \tag{18}$$

where

$$\langle \bullet \rangle = \sum_{s=1}^{N_L} \int_{x_3(s-1)}^{x_3(s)} (\bullet) dx_3 \tag{19}$$

The virtual work done by the inertial forces is given by

$$\delta W_{in} = -\int_{\Omega_m} \left\langle \rho \ddot{\tilde{\mathbf{d}}}^T \delta \tilde{\mathbf{d}} \right\rangle d\Omega \tag{20}$$

where $\rho(x_3)$ is the material mass density; the over dot indicates differentiation with respect to time, and an overbar the prescribed value of a quantity (for static problems, $\delta W_{in} = 0$).

The virtual work done by the applied transverse pressure $\bar{q}_z$ (with reference to the plate's mid-plane), and the transverse load (per unit-length) $\bar{F}_z$ applied along the plate's edge (see Figure 1) is given by

$$\delta W_{ext} = \int_{\Omega_m} \bar{q}_z \delta w d\Omega + \int_{\Gamma} \bar{F}_z \delta w ds \tag{21}$$

It is also assumed that the top and bottom surfaces of the plate are free of shear tractions.

Substituting Eqs. (9), (10) and (14) into Eq. (18), the internal virtual work takes on the form

$$\delta U = \int_{\Omega_m} \left\langle \delta \tilde{\boldsymbol{\varepsilon}}_p^{(k)T} \tilde{\boldsymbol{\sigma}}_p^{(k)} + \delta \tilde{\boldsymbol{\gamma}}^{(k)T} \tilde{\boldsymbol{\sigma}}_t^{(k)} \right\rangle d\Omega = \int_{\Omega_m} \delta \left(\boldsymbol{\nabla}_\varepsilon \mathbf{d} \right)^T \mathbf{R} d\Omega \tag{22}$$

where

$$\mathbf{R} = \left\langle \mathbf{Z}_\varepsilon^T \tilde{\boldsymbol{\sigma}} \right\rangle \tag{23}$$

is the vector of the stress and moment stress resultants for unit length,

$$\mathbf{R}^T = \begin{bmatrix} \mathbf{N}^T & \mathbf{M}^T & \mathbf{M}^{(\phi)\mathrm{T}} & \mathbf{T}^T & \mathbf{T}^{(\phi)T} \end{bmatrix} \tag{24}$$

$$\left(\mathbf{N}, \mathbf{M}, \mathbf{M}^{(\phi)} \right) = \left(\begin{Bmatrix} N_{11} \\ N_{22} \\ N_{12} \end{Bmatrix}, \begin{Bmatrix} M_{11} \\ M_{22} \\ M_{12} \end{Bmatrix}, \begin{Bmatrix} M_{11}^{(\phi)} \\ M_{22}^{(\phi)} \\ M_{12}^{(\phi)} \\ M_{21}^{(\phi)} \end{Bmatrix} \right) = \left\langle \left(1, z, \boldsymbol{\Phi}^{(k)} \right) \tilde{\boldsymbol{\sigma}}_p^{(k)} \right\rangle \tag{25}$$

$$\left(\mathbf{T}, \mathbf{T}^{(\phi)} \right) = \left(\begin{Bmatrix} T_1 \\ T_2 \end{Bmatrix}, \begin{Bmatrix} T_1^{(\phi)} \\ T_2^{(\phi)} \end{Bmatrix} \right) = \left\langle \left(1, \boldsymbol{\beta}^{(k)} \right) \tilde{\boldsymbol{\sigma}}_t \right\rangle \tag{26}$$

Substituting Eqs. (12) and (15) in Eq. (23) and by taking into account (10), yields the plate constitutive equations

$$\mathbf{R} = \left\langle \mathbf{Z}_{\boldsymbol{\varepsilon}}^T \begin{bmatrix} \bar{\mathbf{Q}}_p & \mathbf{0} \\ \mathbf{0} & \bar{\mathbf{Q}}_t \end{bmatrix} \mathbf{Z}_{\boldsymbol{\varepsilon}} \right\rangle \boldsymbol{\varepsilon} = \mathbf{S}\boldsymbol{\varepsilon} = \mathbf{S}\left(\nabla_{\boldsymbol{\varepsilon}}\mathbf{d}\right) \tag{27}$$

With

$$\mathbf{S} = \left\langle \mathbf{Z}_{\boldsymbol{\varepsilon}}^T \begin{bmatrix} \bar{\mathbf{Q}}_p & \mathbf{0} \\ \mathbf{0}^T & \bar{\mathbf{Q}}_t \end{bmatrix} \mathbf{Z}_{\boldsymbol{\varepsilon}} \right\rangle = \begin{bmatrix} \mathbf{A} & \mathbf{B} & \mathbf{A}_\phi & \mathbf{0} & \mathbf{0} \\ \mathbf{B} & \mathbf{D} & \mathbf{B}_\phi & \mathbf{0} & \mathbf{0} \\ \mathbf{A}_\phi^T & \mathbf{B}_\phi^T & \mathbf{D}_\phi & \mathbf{0} & \mathbf{0} \\ \mathbf{0} & \mathbf{0} & \mathbf{0} & \mathbf{A}_t & \mathbf{B}_t^\phi \\ \mathbf{0} & \mathbf{0} & \mathbf{0} & \mathbf{B}_t^{\phi T} & \mathbf{D}_t^\phi \end{bmatrix} \tag{28}$$

$$\begin{aligned} &\left(\mathbf{A},\mathbf{B},\mathbf{D}\right) = \left\langle (1,z,z^2)\bar{\mathbf{Q}}_p^{(k)} \right\rangle,\ \left(\mathbf{A}_\phi,\mathbf{B}_\phi,\mathbf{D}_\phi\right) = \left\langle \left(1,z,\boldsymbol{\Phi}^{(k)T}\right)\bar{\mathbf{Q}}_p^{(k)}\boldsymbol{\Phi}^{(k)} \right\rangle \\ &\left(\mathbf{A}_t,\mathbf{B}_t^\phi\right) = \left\langle \left(1,\boldsymbol{\beta}^{(k)}\right)\bar{\mathbf{Q}}_t^{(k)} \right\rangle,\ \mathbf{D}_t^\phi = \left\langle \boldsymbol{\beta}^{(k)T}\bar{\mathbf{Q}}_t^{(k)}\boldsymbol{\beta}^{(k)} \right\rangle \end{aligned} \tag{29}$$

Substituting Eq. (1) into Eq. (20) yields

$$\delta W_{in} = -\int_{\Omega_m} \delta\mathbf{d}^T \mathbf{m}\ddot{\mathbf{d}} d\Omega \tag{30}$$

where

$$\mathbf{m} = \left\langle \rho\mathbf{Z}^T\mathbf{Z} \right\rangle = \begin{bmatrix} \mathbf{m}^{(0)} & \mathbf{0} & \mathbf{m}^{(1)} & \mathbf{m}_\phi^{(0)} \\ \mathbf{0}^T & m^{(0)} & \mathbf{0}^T & \mathbf{0}^T \\ \mathbf{m}^{(1)T} & \mathbf{0} & \mathbf{m}^{(2)} & \mathbf{m}_\phi^{(1)} \\ \mathbf{m}_\phi^{(0)T} & \mathbf{0} & \mathbf{m}_\phi^{(1)T} & \mathbf{m}_\phi^{(2)} \end{bmatrix} \tag{31}$$

$$\left(\mathbf{m}^{(0)},\mathbf{m}^{(1)},\mathbf{m}^{(2)},\mathbf{m}_\phi^{(0)},\mathbf{m}_\phi^{(1)},\mathbf{m}_\phi^{(2)}\right) = \left\langle \rho(\mathbf{I},z\mathbf{I},z^2\mathbf{I},\boldsymbol{\phi}^{(k)},z\boldsymbol{\phi}^{(k)},\boldsymbol{\phi}^{(k)T}\boldsymbol{\phi}^{(k)} \right\rangle \tag{32}$$

Due to the difficulty to obtain closed-form solutions, we search for an approximate solution.

3. Finite element formulation

The accuracy of the finite element solution depends on the ability of the assumed shape functions to accurately model the deformation modes of the structure.

In the following Sections, C^0 quadrilateral plate elements are presented using the displacement approach in conjunction with RZT summarized in the previous Section. More specifically, the constrained technique in conjunction with an appropriate Element Shear Correction (ESC) factor can solve the *shear-locking* problem.

3.1 Discretized equations of motion

Let us consider a quadrilateral plate element with NN surrounding nodes. A generic four-node (NN=4) and a generic eight-node (NN=8) quadrilateral plate element is shown in Figure 3. The reference plane is the physical plane (x_1, x_2). From a computational point of view, each element can be mapped in a conventional square element on the natural plane (ξ, η) where $(\xi, \eta) \in [-1,1]$, thus the numerical integration using the Gaussian quadrature can be easily implemented.

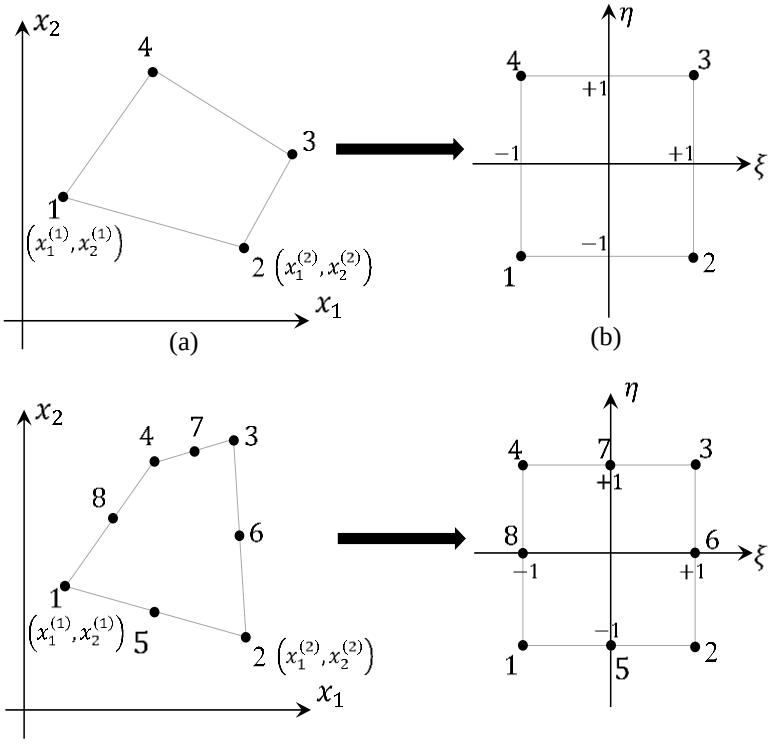

Figure 3 - Four-node and eight-node quadrilateral plate element in physical plane (a) and in natural plane (b).

The element kinematic variables in Eq. (5) can be expressed in the usual manner in terms of the shape functions $\mathbf{N}^{(e)}(\xi, \eta)$ and nodal degrees-of-freedom $\mathbf{q}^{(e)}(t)$, as

$$\mathbf{d}^{(e)}(\xi, \eta; t) = \mathbf{N}^{(e)}(\xi, \eta)\mathbf{q}^{(e)}(t) \tag{33}$$

In expanded form, these relations are given by

$$\mathbf{d}^{(e)}(\xi,\eta)=\begin{Bmatrix}\mathbf{d}_m\\ w^{(0)}\\ \mathbf{d}_r\end{Bmatrix}^{(e)}=\mathbf{N}^{(e)}\mathbf{q}^{(e)}=\begin{bmatrix}\mathbf{N}_m & \mathbf{0} & \mathbf{0}\\ \mathbf{0} & \mathbf{N}_w & \mathbf{0}\\ \mathbf{0} & \mathbf{0} & \mathbf{N}_r\end{bmatrix}^{(e)}\begin{Bmatrix}\mathbf{q}_m\\ \mathbf{q}_w\\ \mathbf{q}_r\end{Bmatrix}^{(e)}$$

$$=\begin{Bmatrix}\mathbf{d}_{u_1}\\ \mathbf{d}_{u_2}\\ w^{(0)}\\ \mathbf{d}_{\theta_1}\\ \mathbf{d}_{\theta_2}\\ \mathbf{d}_{\psi_1}\\ \mathbf{d}_{\psi_2}\end{Bmatrix}^{(e)}=\begin{bmatrix}\mathbf{N}_{u_1} & \mathbf{0} & \mathbf{0} & \mathbf{0} & \mathbf{0} & \mathbf{0} & \mathbf{0}\\ \mathbf{0} & \mathbf{N}_{u_2} & \mathbf{0} & \mathbf{0} & \mathbf{0} & \mathbf{0} & \mathbf{0}\\ \mathbf{0} & \mathbf{0} & \mathbf{N}_w & \mathbf{0} & \mathbf{0} & \mathbf{0} & \mathbf{0}\\ \mathbf{0} & \mathbf{0} & \mathbf{0} & \mathbf{N}_{\theta_1} & \mathbf{0} & \mathbf{0} & \mathbf{0}\\ \mathbf{0} & \mathbf{0} & \mathbf{0} & \mathbf{0} & \mathbf{N}_{\theta_2} & \mathbf{0} & \mathbf{0}\\ \mathbf{0} & \mathbf{0} & \mathbf{0} & \mathbf{0} & \mathbf{0} & \mathbf{N}_{\psi_1} & \mathbf{0}\\ \mathbf{0} & \mathbf{0} & \mathbf{0} & \mathbf{0} & \mathbf{0} & \mathbf{0} & \mathbf{N}_{\psi_2}\end{bmatrix}^{(e)}\begin{Bmatrix}\mathbf{q}_{u_1}\\ \mathbf{q}_{u_2}\\ \mathbf{q}_w\\ \mathbf{q}_{\theta_1}\\ \mathbf{q}_{\theta_2}\\ \mathbf{q}_{\psi_1}\\ \mathbf{q}_{\psi_2}\end{Bmatrix}^{(e)} \tag{34}$$

where $\mathbf{q}_i^{(e)}(t)$ $(i\equiv u_1,u_2,w,\theta_1,\theta_2,\psi_1,\psi_2)$.

Substituting Eq. (33) into Eqs. (22) and (30), yields

$$\delta U^{(e)}=\delta\mathbf{q}^{(e)T}\mathbf{K}^{(e)}\mathbf{q}^{(e)} \tag{35}$$

$$\delta W_{in}^{(e)}=-\delta\mathbf{q}^{(e)T}\mathbf{M}^{(e)}\ddot{\mathbf{q}}^{(e)} \tag{36}$$

$$\delta W_{ext}^{(e)}=\delta\mathbf{q}^{(e)T}\mathbf{P}^{(e)} \tag{37}$$

where the element stiffness and mass matrices are given by

$$\mathbf{K}^{(e)}=\int_{-1}^{+1}\int_{-1}^{+1}\left(\nabla_\varepsilon\mathbf{N}^{(e)}\right)^T\mathbf{S}^{(e)}\left(\nabla_\varepsilon\mathbf{N}^{(e)}\right)Jd\xi d\eta \tag{38}$$

$$\mathbf{M}^{(e)}=\int_{-1}^{+1}\int_{-1}^{+1}\mathbf{N}^{(e)T}\mathbf{m}^{(e)}\mathbf{N}^{(e)}Jd\xi d\eta \tag{39}$$

and the consistent load vector has the form

$$\mathbf{P}^{(e)T}=\int_{-1}^{+1}\int_{-1}^{+1}\begin{bmatrix}\mathbf{0} & \mathbf{0} & \mathbf{N}_w^{(e)} & \mathbf{0} & \mathbf{0} & \mathbf{0} & \mathbf{0}\end{bmatrix}^T\bar{q}_z Jd\xi d\eta+\int_{\Gamma_p^{(e)}}\begin{bmatrix}\mathbf{0} & \mathbf{0} & \mathbf{N}_w^{(e)} & \mathbf{0} & \mathbf{0} & \mathbf{0} & \mathbf{0}\end{bmatrix}^T\bar{F}_z\,d\Gamma \tag{40}$$

where the transverse load (per unit-length) $\bar{F}_z$ if applied along the element's edges gives

$$\int_{\Gamma_p^{(e)}}\bar{F}_z\,\mathbf{N}_w^{(e)T}d\Gamma=\frac{a^{(e)}}{2}\int_{-1}^{+1}\left(\bar{F}_{23}(\xi,-1)\mathbf{N}_w^{(e)T}(\xi,-1)+\bar{F}_{23}(\xi,1)\mathbf{N}_w^{(e)T}(\xi,1)\right)d\xi+$$
$$+\frac{b^{(e)}}{2}\int_{-1}^{+1}\left(\bar{F}_{13}(-1,\eta)\mathbf{N}_w^{(e)T}(-1,\eta)+\bar{F}_{13}(1,\eta)\mathbf{N}_w^{(e)T}(1,\eta)\right)d\eta \tag{41}$$

where J denotes the determinant of the Jacobian matrix.

Substituting Eq. (35), (36) and (37) into Eq. (17), taking into account that the virtual variations are arbitrary independent variations, yields the following ***equations of motion for the element (e)***

$$\mathbf{M}^{(e)}\ddot{\mathbf{q}}^{(e)} + \mathbf{K}^{(e)}\mathbf{q}^{(e)} = \mathbf{P}^{(e)} \tag{42}$$

For the static problems, Eq. (42) reduces to

$$\mathbf{K}^{(e)}\mathbf{q}^{(e)} = \mathbf{P}^{(e)} \tag{43}$$

And for free vibration problems

$$\mathbf{M}^{(e)}\ddot{\mathbf{q}}^{(e)} + \mathbf{K}^{(e)}\mathbf{q}^{(e)} = \mathbf{0} \tag{44}$$

3.2 Shape functions and the interpolation strategy

From the variational statement used to derive the element governing equation, Eq. (17), only the first derivatives of the kinematic variables appear in the virtual variation of the strain energy expression. To formulate consistent finite elements, for RZT, only C^0 continuous shape functions are required.

The first two elements are the isoparametric quadrilateral plate elements: the RZTQ4 and the RZTQ8. RZTQ4 is a four-node element with bi-linear shape functions; RZTQ8 is an eight-node element with bi-quadratic, otherwise known as serendipity, shape functions. Each node has seven dof's: 3 displacements (u_1, u_2, w), two bending rotations (θ_1, θ_2) and two amplitudes of the zigzag functions, (ψ_1, ψ_2) (see, Table 1). For these elements, the same set of shape functions is used for approximating all the generalized displacements vector,

$$\mathbf{N}_{u_1}^{(e)} = \mathbf{N}_{u_2}^{(e)} = \mathbf{N}_{w}^{(e)} = \mathbf{N}_{\theta_1}^{(e)} = \mathbf{N}_{\theta_2}^{(e)} = \mathbf{N}_{\psi_1}^{(e)} = \mathbf{N}_{\psi_2}^{(e)} \tag{45}$$

The behaviour of RZTQ4 and RZTQ8 has been deeply investigated by Di Sciuva and Sorrenti [41] and these elements exhibit the transverse shear-locking effect when applied to model thin and very thin plates. The improvements to alleviate this undesirable effect are the *anisoparametric* interpolation and the *anisoparametric constrained-edge* strategies. These have been analysed and compared in Ref. [41]. The developed *anisoparametric constrained* element by Di Sciuva and Sorrenti [41], here called ZQ4, is used in next Section as base for a further improvement to avoid the transverse shear-locking effect.

Appendix A gives details of the quadrilateral *unconstrained anisoparametric element* and the *edge-constrained* technique to obtain the ZQ4 element.

Furthermore, the ZQ4 element has bi-linear shape functions for all the variables, with a modification for the transverse displacement in which appear coupling contributes with the bending rotation and spatial amplitude dof's. Eq. (46) gives the shape functions matrix for the ZQ4 element.

$$\mathbf{N}^{(e)} = \begin{bmatrix} \mathbf{N}_L & \mathbf{0} & \mathbf{0} & \mathbf{0} & \mathbf{0} & \mathbf{0} & \mathbf{0} \\ \mathbf{0} & \mathbf{N}_L & \mathbf{0} & \mathbf{0} & \mathbf{0} & \mathbf{0} & \mathbf{0} \\ \mathbf{0} & \mathbf{0} & \mathbf{N}_L & \mathbf{S}_{\theta 1} & \mathbf{S}_{\theta 2} & \mathbf{S}_{\psi_1} & \mathbf{S}_{\psi_2} \\ \mathbf{0} & \mathbf{0} & \mathbf{0} & \mathbf{N}_L & \mathbf{0} & \mathbf{0} & \mathbf{0} \\ \mathbf{0} & \mathbf{0} & \mathbf{0} & \mathbf{0} & \mathbf{N}_L & \mathbf{0} & \mathbf{0} \\ \mathbf{0} & \mathbf{0} & \mathbf{0} & \mathbf{0} & \mathbf{0} & \mathbf{N}_L & \mathbf{0} \\ \mathbf{0} & \mathbf{0} & \mathbf{0} & \mathbf{0} & \mathbf{0} & \mathbf{0} & \mathbf{N}_L \end{bmatrix} \tag{46}$$

3.3 Element-appropriate shear correction (ESC) factor for RZT elements

By advancing the concept of Element-appropriate Shear Correction (ESC) factors, Tessler and Hughes [50,51] developed a number of effective Timoshenko and Mindlin elements that are devoid of shear locking. To derive such element factors (element-dependent coefficients that multiply the transverse-shear strains), the authors used the Strain Energy Matching approach (herein referred as SEM). Although especially effective to model laminated composite structures, the recently developed RZT elements (RZTQ4, RZTQ8, and ZQ4), Di Sciuva and Sorrenti [41], have been shown to suffer from shear locking in the thin regime. To resolve the shear locking deficiency of these elements, the SEM approach is applied herein to derive the ESC factors for RZT elements. Specifically, the new ESC factors will be applied to the ZQ4 element. The new element will be referred to as ZQ4c.

Consider a plate which is discretized using N_{E} plate finite elements. Each element has the strain energy, $U^{(e)}$, which is composed of the bending strain energy, $U_b^{(e)}$, and the transverse shear strain energy, $U_s^{(e)}$, i.e.,

$$U^{(e)} = U_b^{(e)} + U_s^{(e)} \tag{47}$$

The classical shear correction factor used in FSDT multiply the transverse shear stiffness coefficient. We consider a quadrilateral ZQ4 element and in this case, we multiply the element shear forces resultants with the element-appropriate shear correction factor $\phi_{(e)}^2$ to correct the solution from the shear-locking error:

$$\breve{\mathbf{T}}^{(e)} = \begin{Bmatrix} \mathbf{T} \\ \mathbf{T}^{(\phi)} \end{Bmatrix}^{(e)} = \phi_{(e)}^2 \begin{bmatrix} \mathbf{A}_t & \mathbf{B}_t^{\phi} \\ \mathbf{B}_t^{\phi T} & \mathbf{D}_t^{\phi} \end{bmatrix} \begin{Bmatrix} \boldsymbol{\gamma}^{(0)} \\ \boldsymbol{\psi} \end{Bmatrix}^{(e)} = \phi_{(e)}^2 \breve{\mathbf{A}}_t \tilde{\boldsymbol{\gamma}}^{(e)} \tag{48}$$

Inverting Eq. (48) we can express the transverse shear strains as follow

$$\tilde{\boldsymbol{\gamma}}^{(e)} = \frac{1}{\phi_{(e)}^2} \breve{\mathbf{A}}_t^{-1} \breve{\mathbf{T}}^{(e)} \tag{49}$$

Substituting the new form of the transverse shear strain (Eq. (49)) into the expression of the strain energy (Eq. (47)) we obtain the new expression of the strain energy of the improved element ZQ4c:

$$U = \sum_{e=1}^{N_E} \left(U_b^{(e)} + \phi_{(e)}^{-2} U_s^{(e)} \right) \tag{50}$$

In Eq. (50) appears the bending strain energy $\left(U_b^{(e)}\right)$ and the corrected transverse shear strain energy $\left(\phi_{(e)}^{-2} U_s^{(e)}\right)$ where the ESC factor $\left(\phi_{(e)}^{-2}\right)$ is yet unknown. It is important to note that the $U_s^{(e)}$ strain energy is the uncorrected one computed using the ZQ4 formulation.

Now we consider the same plate, with the identical mesh pattern. For this plate, we use higher-order elements, that do not require the element shear correction factor and it is supposed that they give the exact strain energy. Thus, we can write:

$$U_{(ho)} = \sum_{e=1}^{N_E} \left(U_{b_{(ho)}}^{(e)} + U_{s_{(ho)}}^{(e)} \right) \tag{51}$$

We enforce the strain energy matching between the strain energy of ZQ4c element and the strain energy coming from the higher-order elements:

$$U_{(ho)} = U \tag{52}$$

Eq. (52) can be read substituting Eqs. (50) and (51):

$$\sum_{e=1}^{N_E} \left(U_{b_{(ho)}}^{(e)} + U_{s_{(ho)}}^{(e)} \right) = \sum_{e=1}^{N_E} \left(U_b^{(e)} + \phi_{(e)}^{-2} U_s^{(e)} \right) \tag{53}$$

Eq. (53) can be rewritten by grouping the two terms under the same summation symbol:

$$\sum_{e=1}^{N_E} \left(U_{b_{(ho)}}^{(e)} - U_b^{(e)} + U_{s_{(ho)}}^{(e)} - \phi_{(e)}^{-2} U_s^{(e)} \right) = 0 \tag{54}$$

The Eq. (54) leads to having N_E independent equations in terms of the N_E unknowns, the element shear correction factors, $\phi_{(e)}^2$.

For each equation, we can write:

$$U_{b_{(ho)}}^{(e)} - U_b^{(e)} + U_{s_{(ho)}}^{(e)} - \phi_{(e)}^{-2} U_s^{(e)} = 0 \tag{55}$$

From Eq. (55) the ESC factor can be easily found:

$$\phi_{(e)}^2 = \left[\frac{U_{s_{(ho)}}^{(e)}}{U_s^{(e)}} + \frac{U_b^{(e)}}{U_s^{(e)}} \left(\frac{U_{b_{(ho)}}^{(e)}}{U_b^{(e)}} - 1 \right) \right]^{-1} \tag{56}$$

Assuming that the higher-order bending and transverse shear strain element energies are proportional to the others, two proportional coefficients can be introduced:

$$U_{b_{(ho)}}^{(e)} = C_{(e)}^b U_b^{(e)}; \qquad U_{s_{(ho)}}^{(e)} = C_{(e)}^s U_s^{(e)} \tag{57}$$

The ratio between the element bending strain energy and the element transverse shear one can be seen as an element material-geometrical parameter, $\alpha_{(e)}$:

$$\alpha_{(e)} = \frac{U_b^{(e)}}{U_s^{(e)}} \tag{58}$$

The element strain energies shown in Eq. (58) are those computed using the ZQ4 formulation. In particular, Eq. (58) can be displayed for the four-node quadrilateral element showing the bending and transverse shear stiffness coefficients.

$$\alpha_{(e)} = \frac{\sum_{i=13}^{28} K_{ii}^s}{\sum_{i=13}^{28} K_{ii}^b} \tag{59}$$

In the $\alpha_{(e)}$ parameter, there are involved the summation of bending and shear stiffness diagonal coefficients associated with the rotational and spatial amplitude degrees of freedom. It should be noted that in Eq. (59) it can be easily found the expression of the material-geometrical parameter of FSDT (see the improved Mindlin three-node element Ref. [51]) if the enhancements of RZT are neglected.

Substituting Eqs. (57) and (58) into Eq. (56), the element shear correction factor can be rewritten:

$$\phi_{(e)}^2 = \left[C_{(e)}^s + \alpha_{(e)} \left(C_{(e)}^b - 1 \right) \right]^{-1} \tag{60}$$

In general, the proportional coefficients $C_{(e)}^s$ and $C_{(e)}^b$ are the same for all the elements, thus it can be used $C_{(e)}^s = C^s$ and $C_{(e)}^b = C^b$. Introducing the new coefficient $C^{-1} = C^b - 1$, Eq. (60) can be rearranged:

$$\phi_{(e)}^2 = \frac{1}{C^s + \alpha_{(e)} / C} \tag{61}$$

In Eq. (61) there are two coefficient that need to be determined. The first one (C^s) can be obtained from the following considerations. When the element is used for very thin plates ($h \to 0$), the $\alpha_{(e)}$ parameter is very high, thus the C^s parameter has little influence on the value of element shear correction factor $\phi^2_{(e)}$. For thick plates, the element correction factor is no needed, because the ZQ4 element works very well as shown by Di Sciuva and Sorrenti [41]. Furthermore, the material-geometrical parameter ($\alpha_{(e)}$) in thick regimes it is expected to have low values. This results in having $\phi^2_{(e)} \to 1/C^s$. To assure the same remarkable accuracy of ZQ4 element for the new ZQ4c element, it needs to have $\phi^2_{(e)} \to 1$ in thick regimes. The only one acceptable value for C^s is $C^s=1$. The other parameter (C) can be determined numerically and its value can be chosen to improve the convergence rate of solution for static and free vibration problems.

Relying on these last considerations, the final form of element shear correction factor is reached:

$$\phi^2_{(e)} = \frac{1}{1+\alpha_{(e)}/C} \tag{62}$$

In Table 1 are resumed the elements herein presented and their main characteristics.

Table 1 – Acronyms, topologies, dof's and shape functions of quadrilateral elements formulated in this study.

Element Type	Nodal Configuration	Degrees of freedom	Shape Functions	Note
RZTQ4	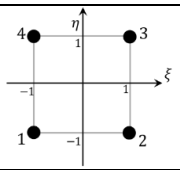	28	Bi-linear Lagrange	-
RZTQ8	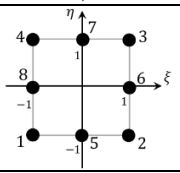	56	Eight-node serendipity	-
ZQ4	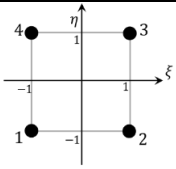	28	Anisoparametric constrained interpolation	Edge constraints Eq. (A.6)
ZQ4c	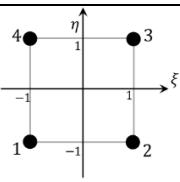	28	Anisoparametric constrained interpolation	Edge constraints Eq. (A.6) + ESC $\left(\phi^2_{(e)}\right)$

4. Numerical results

In order to assess the numerical performances of this new locking free element (ZQ4c) when applied to the linear analysis of bending and free vibration problems for rectangular thick, thin and very thin laminated composite and sandwich plates, several numerical tests have been carried out. The numerical investigation has been conducted on various sample problems for which the analytical solution is available or it can be obtained using the Ritz method as it is implemented by Di Sciuva and Sorrenti [26]. A comparison of the 4 elements (RZTQ4, RZTQ8, ZQ4 and ZQ4c) is made to test the elements regarding the shear locking problem. The behaviour of the new element ZQ4c, convergence rate, ESC effect, global quantities (maximum displacement, fundamental frequency, shear force and bending moment distributions) and local quantities (through-thickness strain and stress distributions) are evaluated considering different boundary and loading conditions. Figure 4 shows the plate dimensions, boundary conditions and load cases considered in this numerical analysis. The letter S refers to simply supported edge, the letter C refers to clamped edge and the letter F refers to free edge. For load acronyms, letter B means bi-sinusoidal load pressure, letter U means uniform load pressure and letter E means constant edge load.

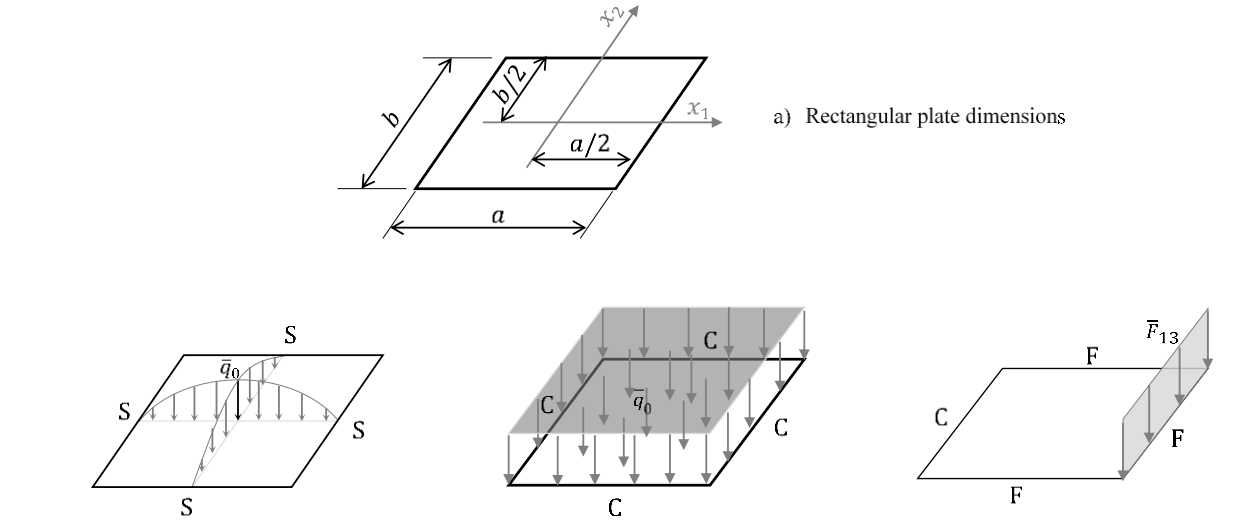

@ $x_1 = \pm\frac{a}{2}$ $\quad u_2 = w = \theta_2 = \psi_2 = 0;$

@ $x_2 = \pm\frac{b}{2}$ $\quad u_1 = w = \theta_1 = \psi_1 = 0$

@ $x_1; x_2 = \pm\frac{a}{2}; \pm\frac{b}{2}$

$u_1 = u_2 = w = \theta_1 = \theta_2 = \psi_1 = \psi_2 = 0$

@ $x_1 = -\frac{a}{2}$

$u_1 = u_2 = w = \theta_1 = \theta_2 = \psi_1 = \psi_2 = 0$

Figure 4 – Rectangular plate dimensions, boundary conditions and load distributions; b) simply supported under bi-sinusoidal load (SSSS-B); c) fully clamped under uniform load pressure (CCCC-U); d) Cantilever under uniform edge load (CFFF-E).

If not otherwise specified, the results presented in this Section refer to center non-dimensional deflection, $\bar{w} = 100\dfrac{h^3 E_2}{\bar{q}_0 a^4} w$

and to the undamped frequency parameter, $\bar{f} = f\dfrac{a^2}{h}\sqrt{\dfrac{\rho}{E_2}}$.

The non-dimensional in-plane displacements and stresses are defined as follows ($\bar{q}_0$ is the maximum intensity of the applied transverse pressure, *a* is the length of the plate *b* is the width, E_2 is Young's modulus in x_2 direction of the first layer)

$$\bar{u}_1 = 100\frac{h^3 E_2}{q_0 a^4} u_1\left(x_1, x_2, z\right); \qquad \left(\bar{\sigma}_{11}, \bar{\sigma}_{22}\right) = \frac{h^2}{q_0 a^2}\left(\sigma_{11}\left(x_1, x_2, z\right), \sigma_{22}\left(x_1, x_2, z\right)\right); \qquad \left(\bar{\sigma}_{13}, \bar{\sigma}_{23}\right) = \frac{h}{\bar{q}_0 a}\left(\sigma_{13}, \sigma_{23}\right)\left(x_1, x_2, z\right)$$

Table 2 gives the mechanical characteristics and material density of the unidirectional layers constituting the laminated composite and sandwich plates investigated in this study, number and thickness of the layers, lamina orientation of the principal material direction 1, material of the single layer, are given in Table 3.

Table 2 - Mechanical characteristics and material density of the unidirectional layers.

	$E_1\ [MPa]$	$E_2\ [MPa]$	$E_3\ [MPa]$	$G_{12}\ [MPa]$	$G_{13}\ [MPa]$	$G_{23}\ [MPa]$	ν_{12}	ν_{13}	ν_{23}	$\rho\ \left[\frac{Kg}{m^3}\right]$
A	300000	12000	12000	6000	6000	2400	0.25	0.25	0.25	1000
CE	110000	7857	7857	3292	3293	1292	0.33	0.33	0.49	1600
R	40.3	40.3	40.3	12.4	12.4	12.4	0.30	0.30	0.30	60

Table 3 - Laminate composites and sandwich plates.

Laminate Name	$h^{(k)}/h$	Lamina orientation	Materials
L1	0.3333/0.3333/0.3333	0/90/0	A/A/A
L2	0.05/0.05/0.8/0.05/0.05	0/90/core/90/0	CE/CE/R/CE/CE

4.1 RZT analytical performances

The accuracy and reliability of RZT plate theory to predict global and local quantities are here briefly compared with an exact elasticity solution. We consider a symmetric thick (span-to-thickness ratio, *a/h*=5) cross-ply (L1) square plate simply supported on all edges, under bi-sinusoidal transverse pressure of intensity $\bar{q}_0$. Figure 5 shows the thickness-wise distribution of the non-dimensional displacement $\bar{u}_1$, maximum transverse displacement, $\bar{u}_3$, bending stresses, $\bar{\sigma}_{11}$ and $\bar{\sigma}_{22}$, transverse shear stress, $\bar{\sigma}_{13}$ compared with the exact elasticity solution obtained using Pagano approach [56]. RZT, as expected, has remarkable accuracy and does not need any shear correction factor. Furthermore, it is also interesting to note that the linear RZT is very close with the cubic variation of in-plane displacement $\bar{u}_1$, and in-plane stress $\bar{\sigma}_{11}$. Improvements on RZT to consider higher zigzag functions can be used for a better through-the-thickness description and

can be found in the works of Barut et al [57] and Iurlaro et al [58]. Iurlaro et al [34] Sorrenti and Di Sciuva [35] also demonstrated how it is possible using the linear RZT to obtain more complex variations of the previous variables without increase the number of unknowns.

It is also shown that the transverse shear stresses recovered via the equilibrium equations are very close with 3D exact solution. The transverse shear stresses obtained by the constitutive relations are sufficiently accurate in the average sense. In the remaining part of the numerical analysis, for a comparison purpose of new element performance will be considered only the transverse shear stresses obtained from equilibrium equations.

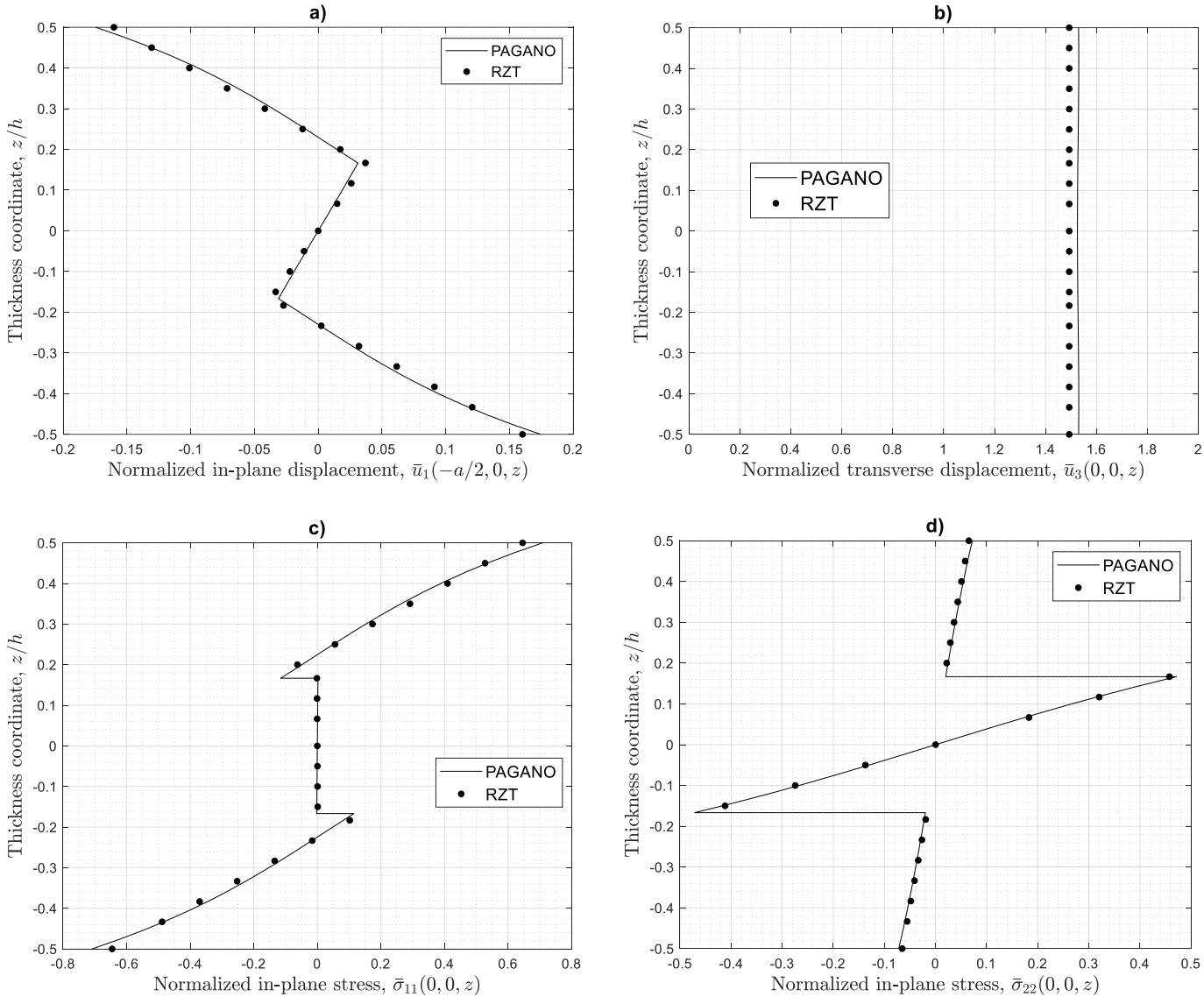

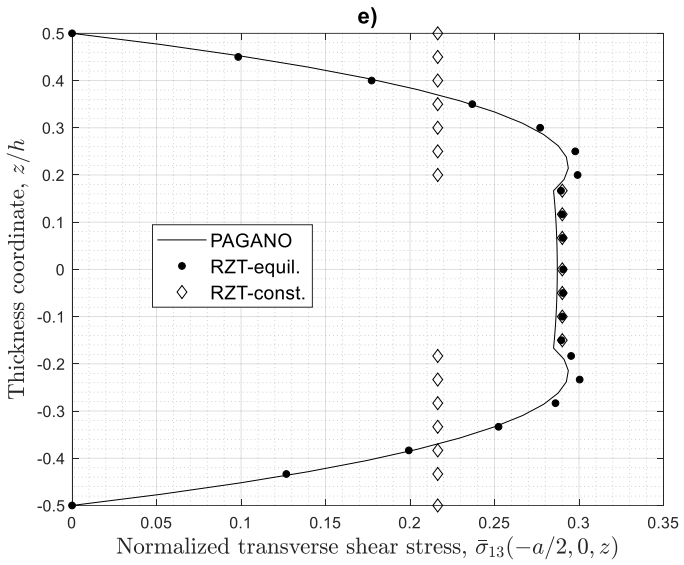

Figure 5 - Bending of a square cross-ply plate (L1), simply supported on all edges under transverse sinusoidal pressure (*a/h=5*); in e) RZT-const. stands for the values evaluated using the constitutive equations and RZT-equil. stands for the values coming from the integration of the local equilibrium equations.

4.2 Shear locking problem

In order to investigate the shear locking phenomenon of the four plate elements, Figure 6 shows the results for the non-dimensional maximum deflection (r_w) as a function of the span-to-thickness ratio (*a/h*). The plate considered is the square cross-ply (L1) plate, simply supported on all edges and under bi-sinusoidal transverse pressure. We consider a regular, i.e. the elements in the physical plane are square, 8x8 mesh (see Figure 9) considering only a quarter of plate. The ZQ4c element uses the numerical coefficient determined in the following subsection 4.3.

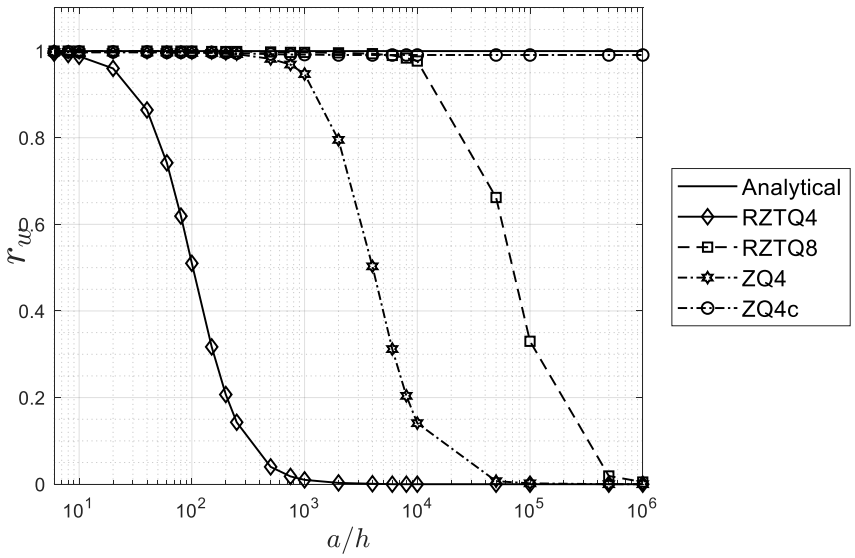

Figure 6 - Non-dimensional maximum displacement vs span-to-thickness ratio for square simply supported cross-ply (L1) plate (8x8 a quarter of plate).

As expected, from Figure 6, the RZTQ4 element has already been affected by the shear locking problem for moderately thin plates (*a/h=50*). RZTQ8 has better results because it has been formulated using bi-quadratic shape functions for all the kinematic variables, but the cost computational is higher than the isoparametric four-node. However, the RZTQ8 element is still affected by shear locking phenomenon. The ZQ4 element, with the constrained technique, has a good behaviour till $a/h=10^3$ but for very thin span-to-thickness ratios the shear-locking effect is very evident. Only the new element ZQ4c with the combination of the constrained technique and the new ESC factor has very good performance, using the full integration, for static problem and all the span-to-thickness ratios considered (from very thick plate to very thin ones).

Because the RZTQ4, the RZTQ8 and ZQ4 elements have been assessed in Ref. [41], in the remaining part of this work we focus our attention to the analysis of this new improved element, the ZQ4c element.

4.3 The role of Element Shear Correction Factor

In this Section, we investigate the properties of the new Element Shear Correction Factor. The ESC factor is depending on the material-geometry parameters, and on the arbitrary coefficient (C) that can improve the convergence rate of the solution, see Eqs. (59) and (62). To use the new ESC factor, it requires an optimal choice for the coefficient C. To obtain this value we compare the errors of strain energy computed using a regular mesh (8x8 elements, a quarter of plate) considering the following cases:

- Simply supported square cross-ply (L1) and sandwich (L2) plates under bi-sinusoidal transverse pressure for $a/h=10^3$
- Fully clamped square cross-ply (L1) and sandwich (L2) plates under uniform pressure for $a/h=10^3$

We define the strain energy error as follows:

$$E_U = \left(\frac{U_{FEM}}{U_{analytical}} - 1 \right) \cdot 100\% \tag{63}$$

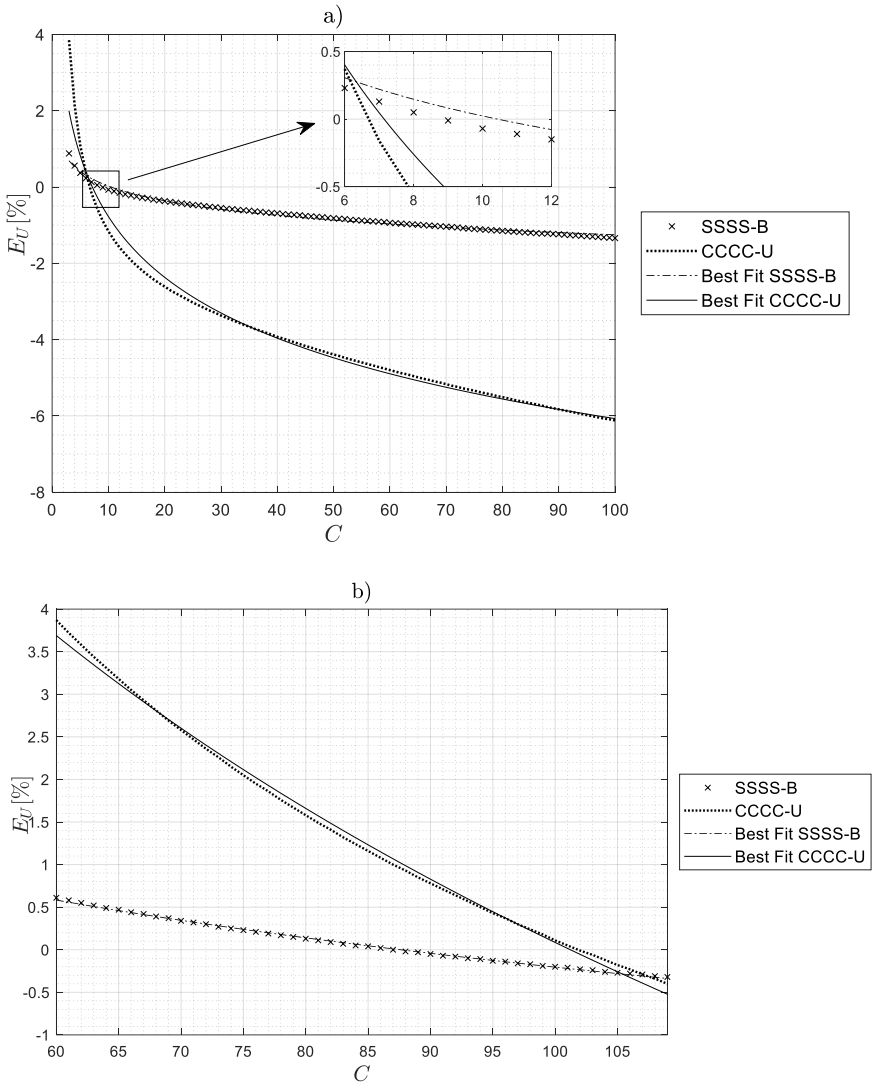

Figure 7 – Percent error of strain energy for thin plates (*a/h=10*^{3}): a) Cross-ply L1 and b) Sandwich L2.

Figure 7 shows the percent errors of the strain energy varying the parameter C. For each case, the best-fit curves are computed using a logarithmic regression. For the cross-ply (L1) plate, the average value is C=8.79, while for the sandwich (L2) plate the average value is C=94.40. A compromise between the two values can be considered as C=50.00 and this value is adopted in the remaining part of the numerical assessment of the ZQ4c element.

Figure 8 shows the influence of the element geometrical and material properties of the element for the ESC, ϕ^2. The behaviour of this new ESC factor is very similar to those presented by Tessler and Hughes [50].

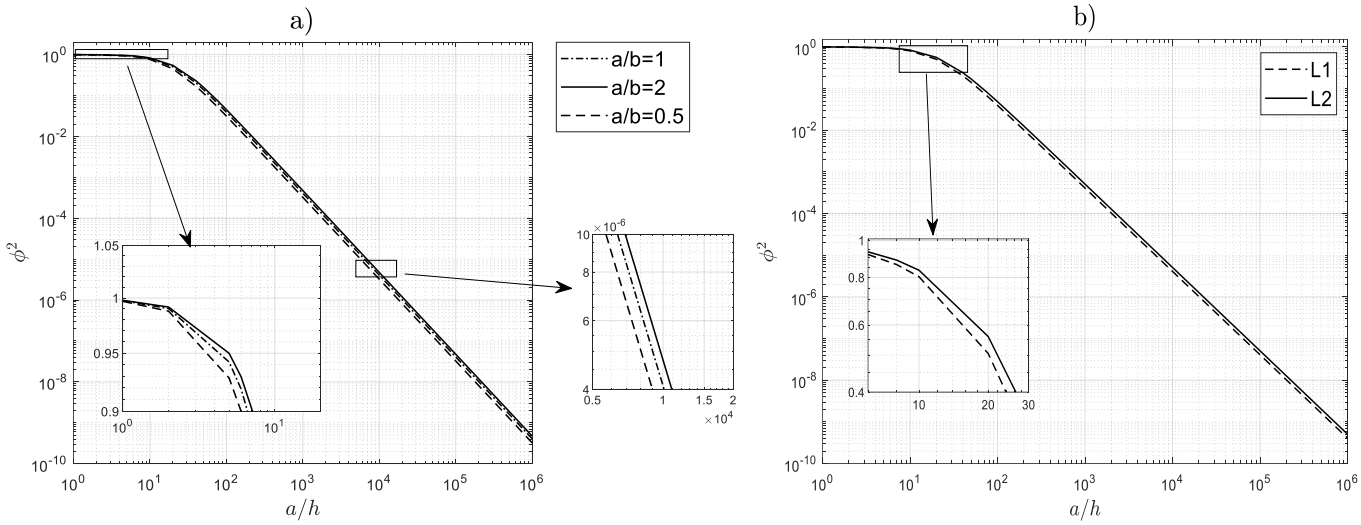

Figure 8 – Element shear correction factor ϕ^2 versus span-to-thickness ratio (*a/h*). a) Effect of element geometry for cross-ply (L1) and b) effect of material properties for laminate L1 and sandwich L2.

4.4 Spectral analysis

The ZQ4c element has the correct rank of stiffness matrix because the "full" gaussian quadrature is used. As expected, no spurious zero-energy modes are present. Also, the other elements, RZTQ4, RZTQ8 and ZQ4, when the full integration is performed no extra spurious energy have seen. Typically, in commercial FEM codes, the Reduced Integration is used to solve the shear locking problem. Even though this solution could solve the shear locking phenomenon it leads to the appearance of the extra zero strain energy modes that need to be solved using appropriate stabilization technique to avoid the *hourglass* effect. Table 4 gives the number of rigid body modes for the various plate elements (3 rigid translations and 3 rigid rotation) expecting for the RZTQ4 with reduced integration, where an extra zero-energy appears.

Table 4 – Number of rigid-body modes

Element	Type of integration	N° of rigid body modes
RZTQ4	Full	6
RZTQ4	Reduced	7
RZTQ8	Full	6
ZQ4	Full	6
ZQ4c	Full	6

4.5 Convergence analysis

In this Section, the convergence of ZQ4c element is investigated considering both static and free vibration problems.

Due to geometry, boundary conditions and loading symmetry with respect to the reference axes, if not otherwise specified, all FEM results have been obtained meshing only one-quarter of the plate with a regular mesh, i.e., all the elements in the physical plane are square elements. Thus, the number of elements indicated below refers to the number of elements along the side of one-quarter of the full-plate. In Figure 8, the mesh discretization used in this analysis.

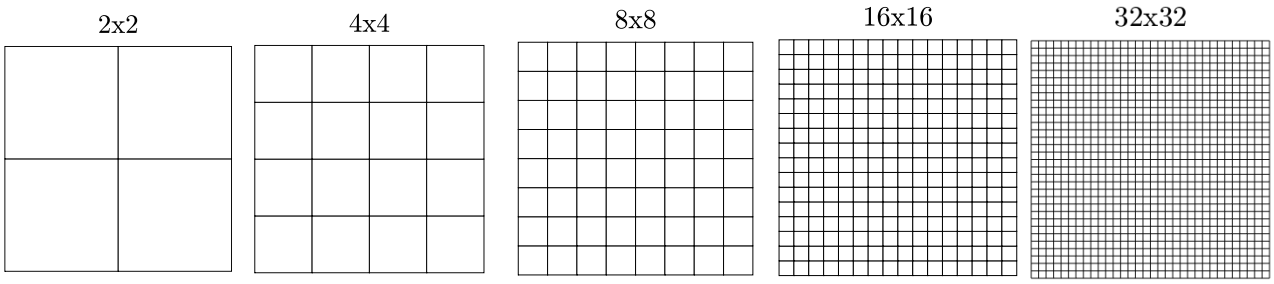

Figure 9 – Regular mesh distributions employed for convergence analysis.

In this analysis, we consider a square cross-ply (L1) plate with various boundary conditions (simply supported and fully clamped plate) and with different load distributions (bi-sinusoidal and uniform transverse pressure).

To show the convergence characteristics of the finite element solution Figures 10 and Figures 11 give plots of the ratios

$$r_w = \frac{\bar{w}_{FEM}}{\bar{w}_{analytic}}; \qquad r_f = \frac{\bar{f}_{FEM}}{\bar{f}_{analytic}}$$

where $(.)_{FEM}$ and $(.)_{analytic}$ stand for the FEM solution and the analytic one, respectively. The analytic solution is obtained with a trigonometric expansion for the simply supported case or using the Ritz method [26] in which 11 Gram-Schmidt functions for the other boundary conditions.

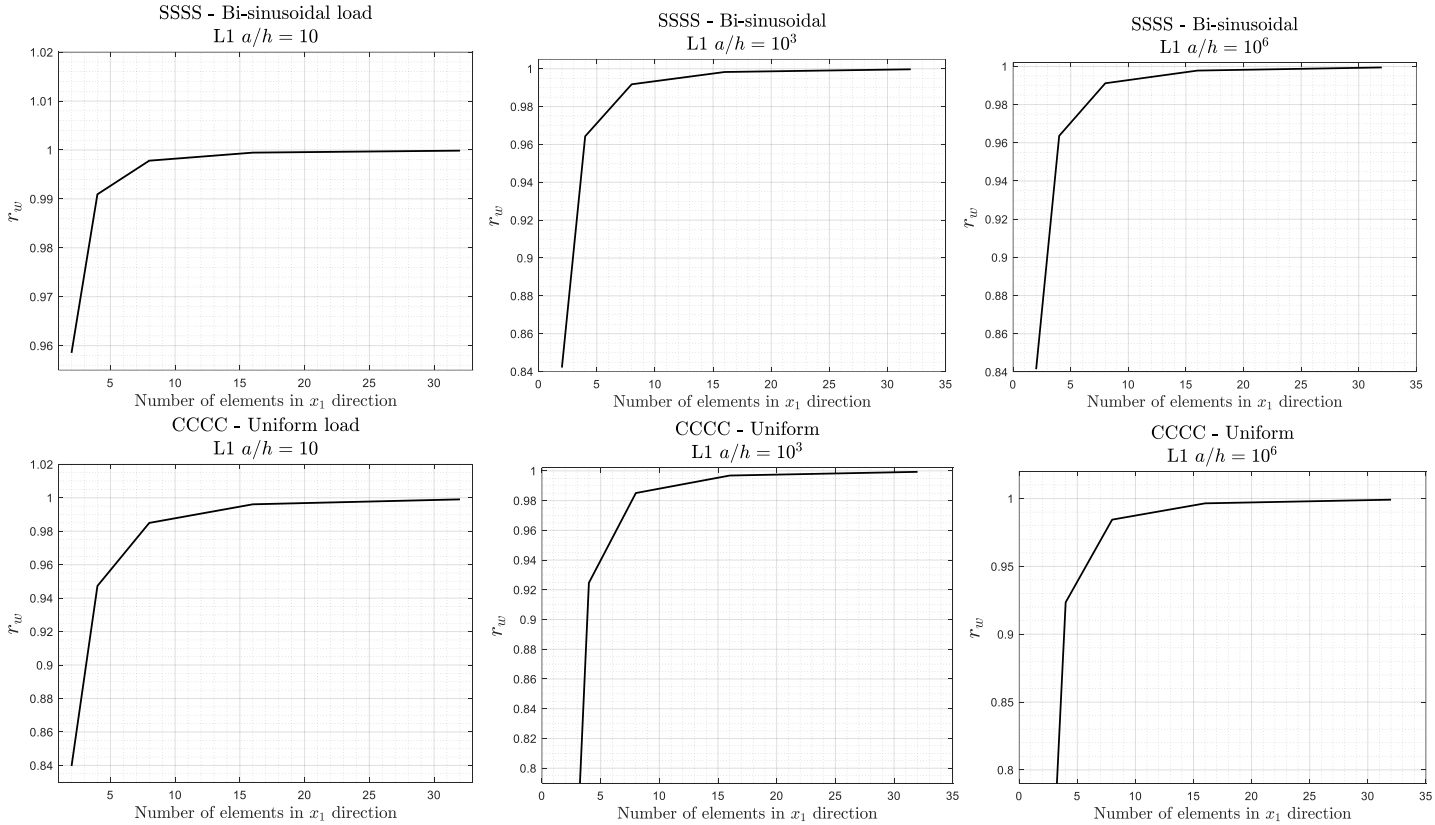

Figure 10 – Convergence results for static problems cross-ply (L1) plate (*a/h=10, a/h=10³, a/h=10⁶*).

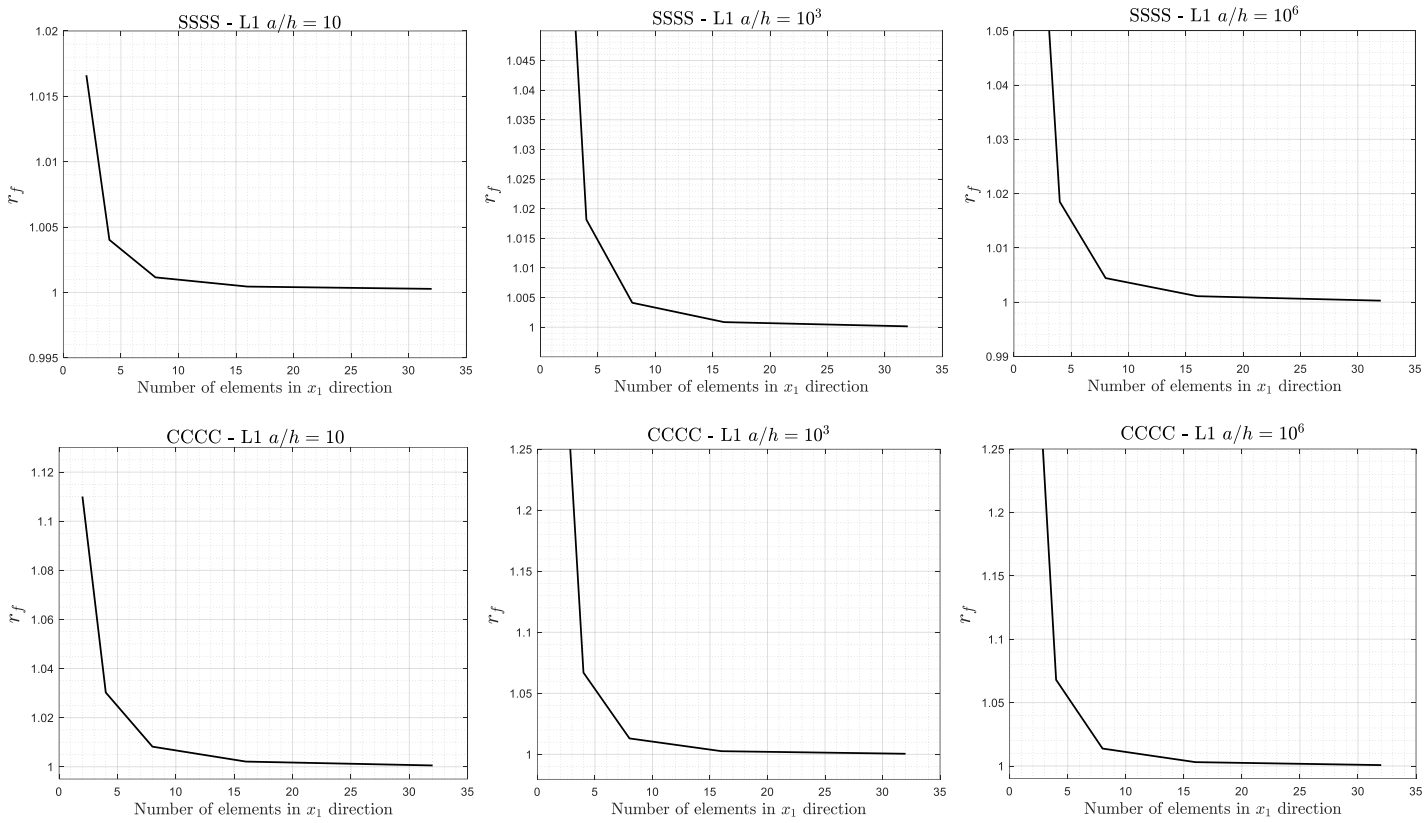

Figure 11 – Convergence results for free vibration. Cross-ply (L1) plate (*a/h=10*, *a/h=10³*, *a/h=10⁶*).

Figures 10 and Figures 11 show good monotonic convergence rates for both static and free undamped vibrations. With an 8x8 mesh pattern, we have very close results with the analytical ones with an error not higher than the 2%. For this reason, the ZQ4c element is very interesting from a computational point of view due to its accuracy with few elements.

Now we consider a rectangular (*a/b=0.5*) cross-ply (L1) plate simply supported under bi-sinusoidal transverse pressure, we analyse the convergence rate for thick plate (*a/h=8*) and for very thin (*a/h=10⁶*) plate. Figure 12 shows the good performance of ZQ4c element to predict the maximum deflection also for rectangular elements guaranteeing an error below 3% also for 4x4 mesh.

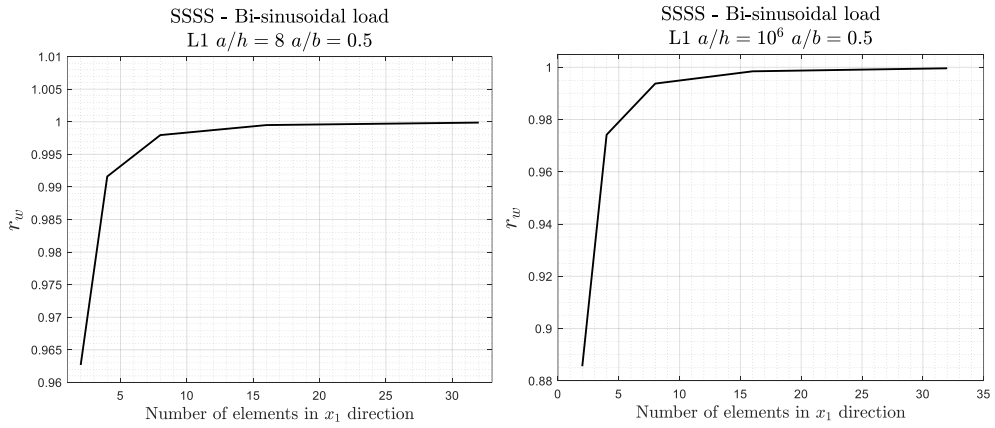

Figure 12 – Convergence rates for rectangular (*a/b=0.5*) cross-ply (L1) plate simply supported under bi-sinusoidal transverse pressure.

We compare the maximum deflection results and the fundamental undamped frequency for square cross-ply (L1) and sandwich (L2) plates considering three combinations of boundary conditions and load cases for various span to thickness ratios:

- Simply supported on all edges under bi-sinusoidal transverse pressure (SSSS-B)
- Fully clamped under uniform transverse pressure (CCCC-U)
- Cantilever and uniform tip edge pressure (CFFF-E)

Table 5 shows the percent errors of maximum deflections and fundamental undamped frequencies defined as

$$err\% = \left(\frac{FEM}{ANALYTICAL} - 1 \right) 100\%$$

The analytical solutions have been obtained using the Ritz method [26] (as shown in Ref. [26], 11 orthogonal polynomials in both x_1 and x_2 directions guarantee the converged Ritz solution). The previous convergence studies, it is shown that 16x16 mesh for a quarter of plate guarantees very accurate results, but in this case, for load conditions motivation, we have to consider a 32x32 mesh for the entire plate.

Table 5 – Percent error of maximum deflection and fundamental undamped frequencies for cross-ply (L1) and sandwich (L2) plates for various span-to-thickness ratios (*a/h*).

	L1						**L2**					
	SSSS-B		**CCCC-U**		**CFFF-E**		**SSSS-B**		**CCCC-U**		**CFFF-E**	
a/h	*w*	*f*	*w*	*w*	*f*	*w*	*w*	*f*	*w*	*f*	*w*	*f*
8	-0.05	0.06	-0.33	0.18	-0.04	0.04	0.00	0.01	-0.28	0.16	-0.05	0.06
10	-0.05	0.04	-0.39	0.21	-0.04	0.04	0.01	0.00	-0.30	0.18	-0.05	0.06
10^2	-0.06	0.03	-0.31	0.19	-0.02	0.02	0.28	-0.14	1.51	-0.30	0.08	-0.06
10^3	-0.17	0.09	-0.32	0.26	-0.02	0.01	0.27	-0.13	1.17	-0.65	0.09	-0.07
10^4	-0.22	0.11	-0.35	0.29	-0.02	0.01	0.23	-0.12	1.09	-0.62	0.09	-0.07
10^6	-0.22	0.11	-0.35	0.30	-0.02	0.01	0.23	-0.11	1.09	-0.62	0.09	-0.06

It is evident that the ZQ4c element is capable to predict with very accuracy the global quantities in the full range of span-to-thickness ratio.

4.6 Regular and distorted mesh analysis

As well know, the performances of the plate finite elements depend also on their skewness ratio, i.e., on the degree of the distortion of their plan form geometry. For this purpose, Figure 13 shows the regular (a) and distorted (b) 16x16 mesh for a quarter of plate. To assess the relative performance of the ZQ4c element when used in distorted geometry, simply

supported and fully clamped square cross-ply (L1) and sandwich (L2) plates under bi-sinusoidal and uniform transverse pressure are considered.

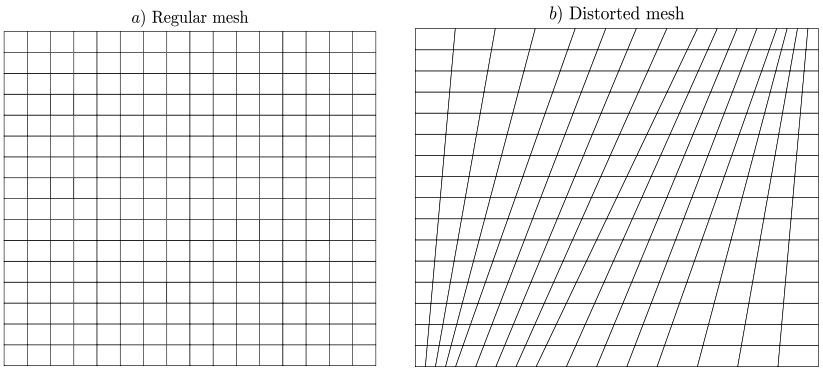

Figure 13 – Regular (a) and distorted (b) 16x16 mesh.

Table 6 gives the percent errors of FEM results on the undamped fundamental frequency parameter for regular and distorted mesh patterns.

Table 6 – Percent errors of FEM results on the maximum deflection and undamped fundamental frequencies for cross-ply (L1) and sandwich (L2) plate regular and distorted 16x16 mesh (Figure 13).

	Regular mesh (16x16)								Distorted mesh (16x16)							
	L1				**L2**				**L1**				**L2**			
	SSSS-B		**CCCC-U**		**SSSS-B**		**CCCC-U**		**SSSS-B**		**CCCC-U**		**SSSS-B**		**CCCC-U**	
a/h	w	f	w	f	w	f	w	f	w	f	w	f	w	f	w	f
6	-0.04	0.08	-0.23	0.14	0.00	0.02	-0.26	0.15	-0.03	0.09	-0.32	0.20	-0.01	0.02	-0.33	0.20
8	-0.05	0.06	-0.33	0.18	0.00	0.01	-0.30	0.16	-0.05	0.07	-0.47	0.26	0.00	0.01	-0.38	0.21
10	-0.05	0.04	-0.39	0.21	0.01	0.00	-0.35	0.18	-0.06	0.06	-0.59	0.32	0.01	0.00	-0.45	0.23
10^2	-0.06	0.03	-0.31	0.19	0.28	-0.14	-0.46	-0.09	-0.09	0.05	-0.50	0.28	0.26	-0.14	-0.60	-0.02
10^3	-0.17	0.09	-0.32	0.26	0.27	-0.13	1.12	-0.64	-0.25	0.16	-0.47	0.37	0.17	-0.09	1.23	-0.71
10^4	-0.22	0.11	-0.35	0.29	0.23	-0.12	1.09	-0.62	-0.30	0.19	-0.51	0.40	0.10	-0.06	1.19	-0.68
10^5	-0.22	0.10	-0.35	0.30	0.23	-0.12	1.09	-0.62	-0.30	0.19	-0.51	0.42	0.10	-0.06	1.19	-0.67
10^6	-0.22	0.11	-0.35	0.30	0.23	-0.11	1.09	-0.62	-0.30	0.19	-0.51	0.42	0.10	-0.06	1.19	-0.67

Very good results are obtained, as expected for regular mesh, and also for distorted mesh, that makes the ZQ4c very competitive not only for its low computational cost but also for its excellent performance under elements distortion.

4.7 Strain and stress distributions

After validation of the ZQ4c elements for global quantities (maximum deflection and undamped fundamental frequency), the local behaviour (strain and stress distributions) is investigated in this Section. A simply supported square cross-ply (L1) plate under bi-sinusoidal transverse pressure is considered. Figure 14 shows the position of the points where the local quantities have been evaluated. We consider only a quarter of plate with a fine mesh of 32x32 elements.

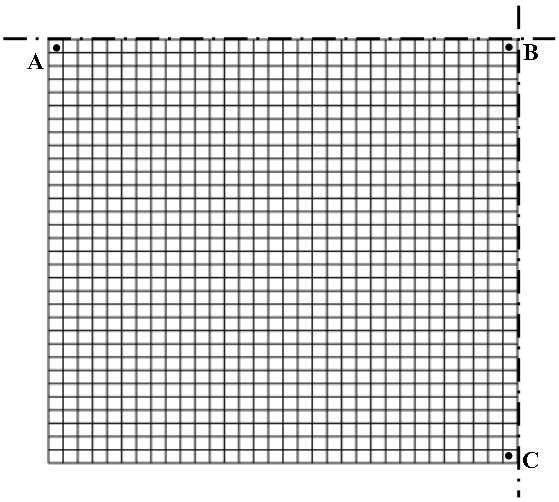

Figure 14 – Points on 32x32 mesh where the local quantities are evaluated.

The corrected values of transverse shear strains are computed from Eq. (48). In particular, the shear element correction factor can be applied directly to the computation of the element transverse shear strain, obtaining the following formulas:

$$\begin{aligned}\gamma_{13}^{(k)(e)} &= \phi_{(e)}^2\left[\mathbf{N}_{L,\xi}\mathbf{q}_w^{(e)} + \left(\mathbf{S}_{\theta_1,\xi} + \mathbf{N}_L\right)\mathbf{q}_{\theta_1}^{(e)} + \mathbf{S}_{\theta_2,\xi}\mathbf{q}_{\theta_2}^{(e)} + \left(\mathbf{S}_{\psi_1,\xi} + \beta_1^{(k)}\mathbf{N}_L\right)\mathbf{q}_{\psi_1}^{(e)} + \mathbf{S}_{\psi_2,\xi}\mathbf{q}_{\psi_2}^{(e)}\right] \\ \gamma_{23}^{(k)(e)} &= \phi_{(e)}^2\left[\mathbf{N}_{L,\eta}\mathbf{q}_w^{(e)} + \mathbf{S}_{\theta_1,\eta}\mathbf{q}_{\theta_1}^{(e)} + \left(\mathbf{S}_{\theta_2,\eta} + \mathbf{N}_L\right)\mathbf{q}_{\theta_2}^{(e)} + \mathbf{S}_{\psi_1,\eta}\mathbf{q}_{\psi_1}^{(e)} + \left(\mathbf{S}_{\psi_2,\eta} + \beta_2^{(k)}\mathbf{N}_L\right)\mathbf{q}_{\psi_2}^{(e)}\right]\end{aligned} \tag{64}$$

In Figures 15, 16, 17 and 18 it is shown the in-plane and transverse shear strains and the non-dimensional stresses as defined previously.

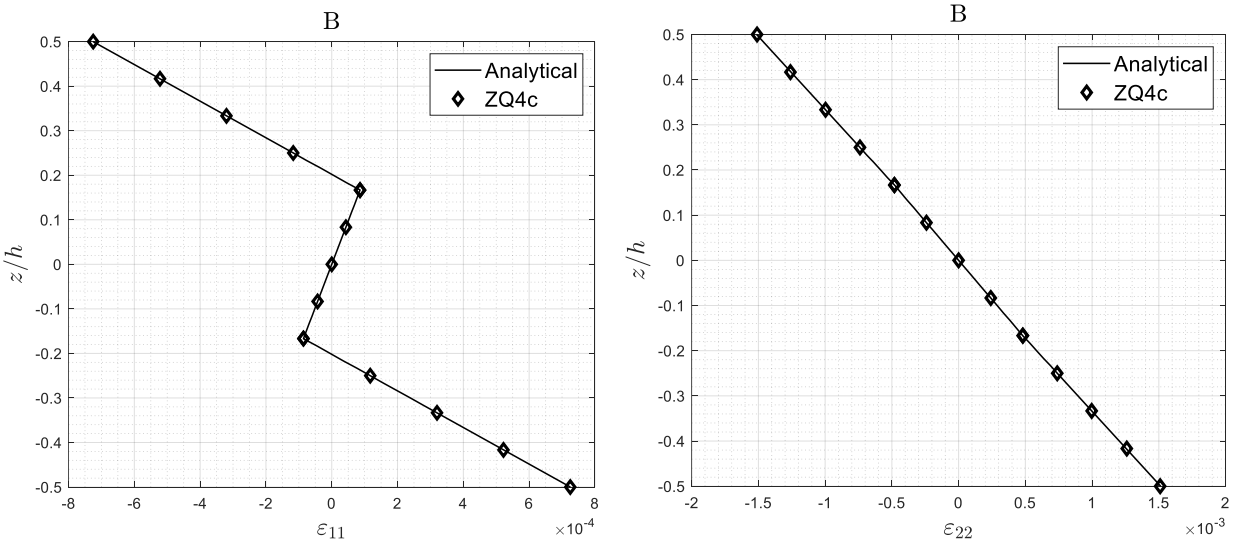

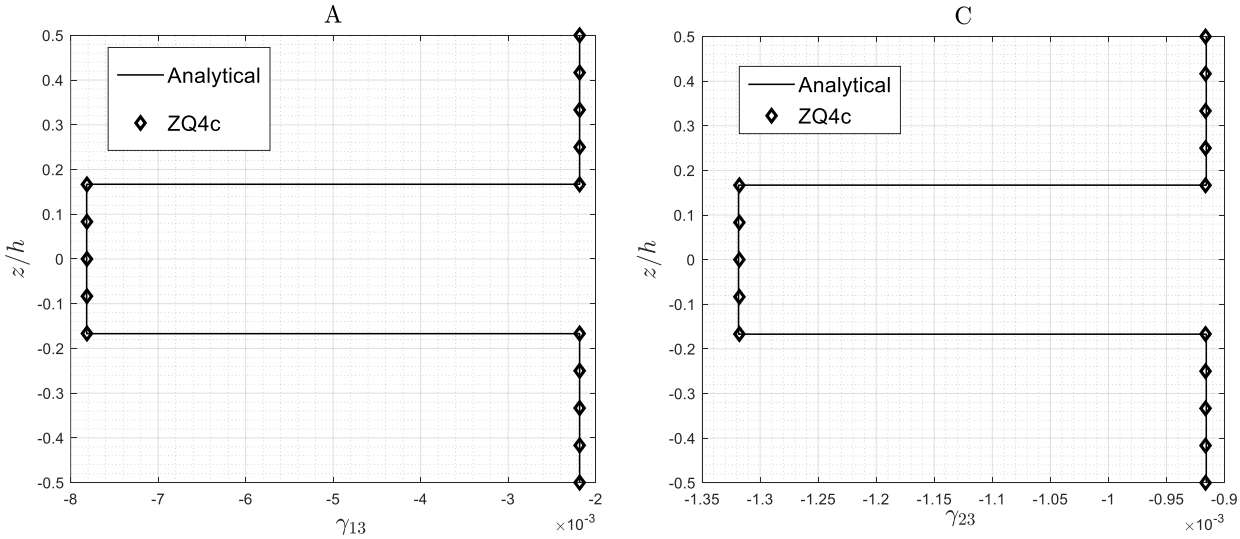

Figure 15 – Strain quantities evaluated in points A, B and C (see Figure 14 for thick (*a*/*h*=6) cross-ply (L1) simply supported square plate under bi-sinusoidal load.

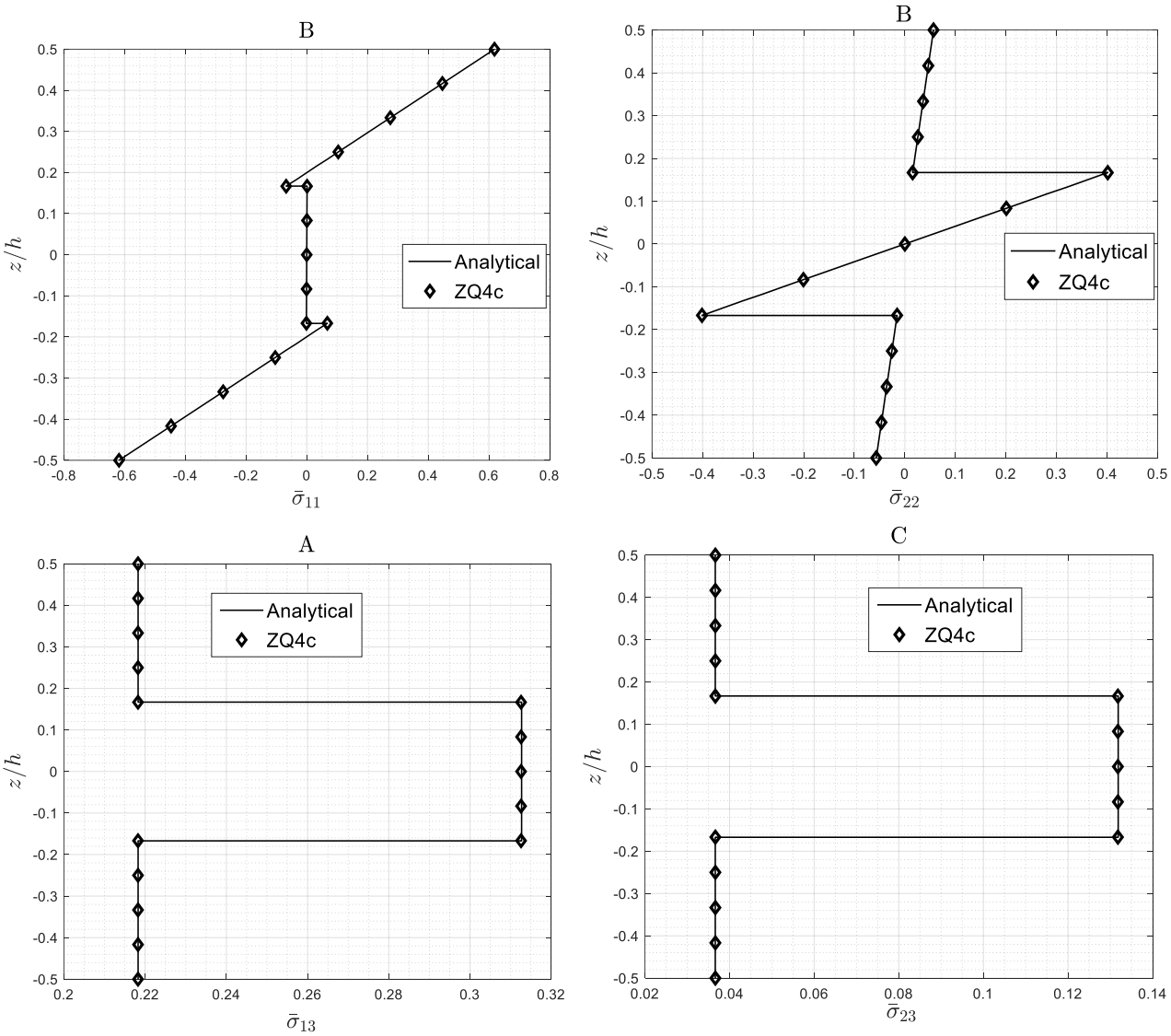

Figure 16 – Stress quantities evaluated in point A, B and C (see Figure 14) for cross-ply (L1) simply supported square plate under bi-sinusoidal load.

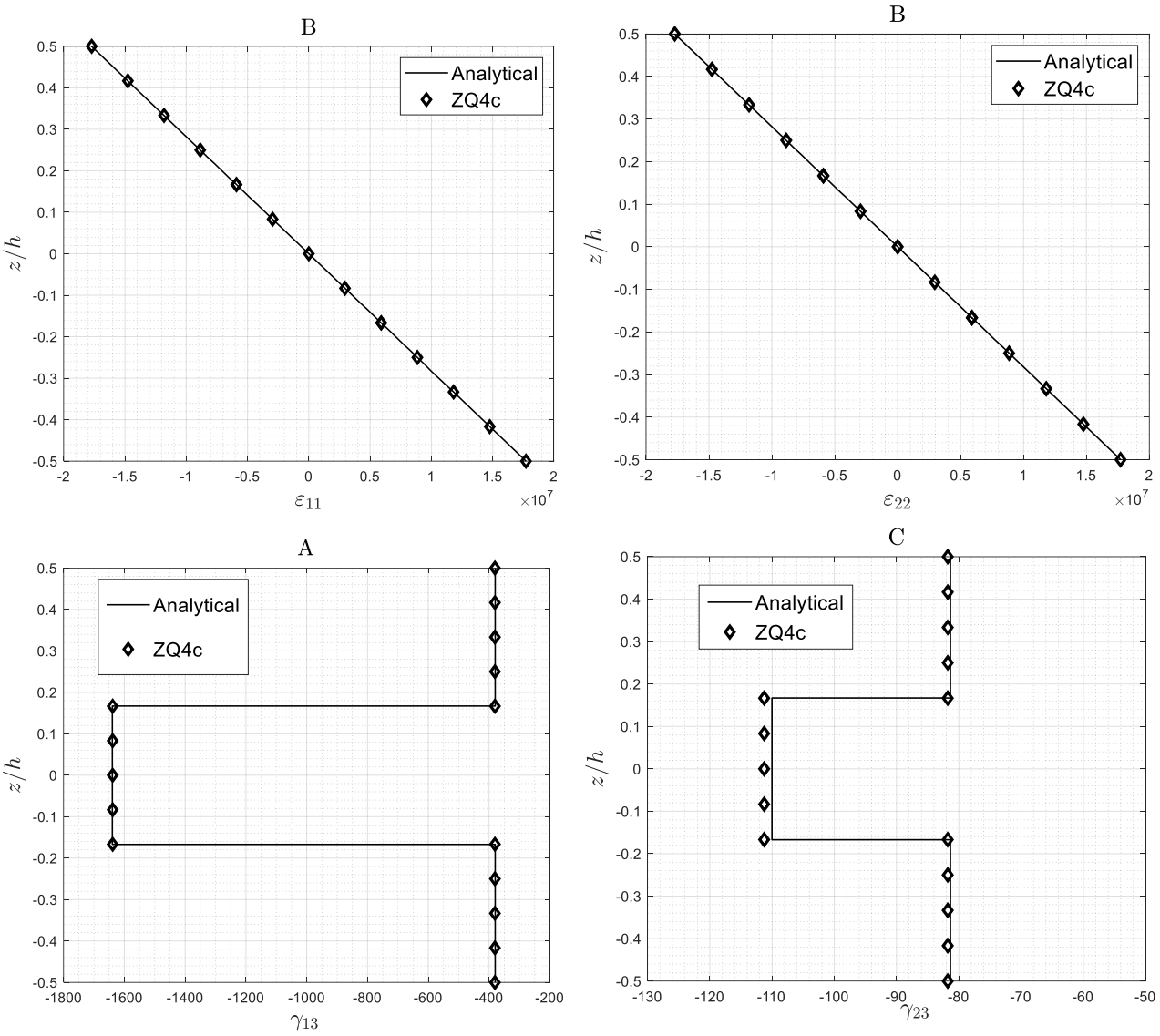

Figure 17 – Strain quantities evaluated in points A, B and C (see Figure 14) for thin ($a/h=10^6$) cross-ply (L1) simply supported square plate under bi-sinusoidal load.

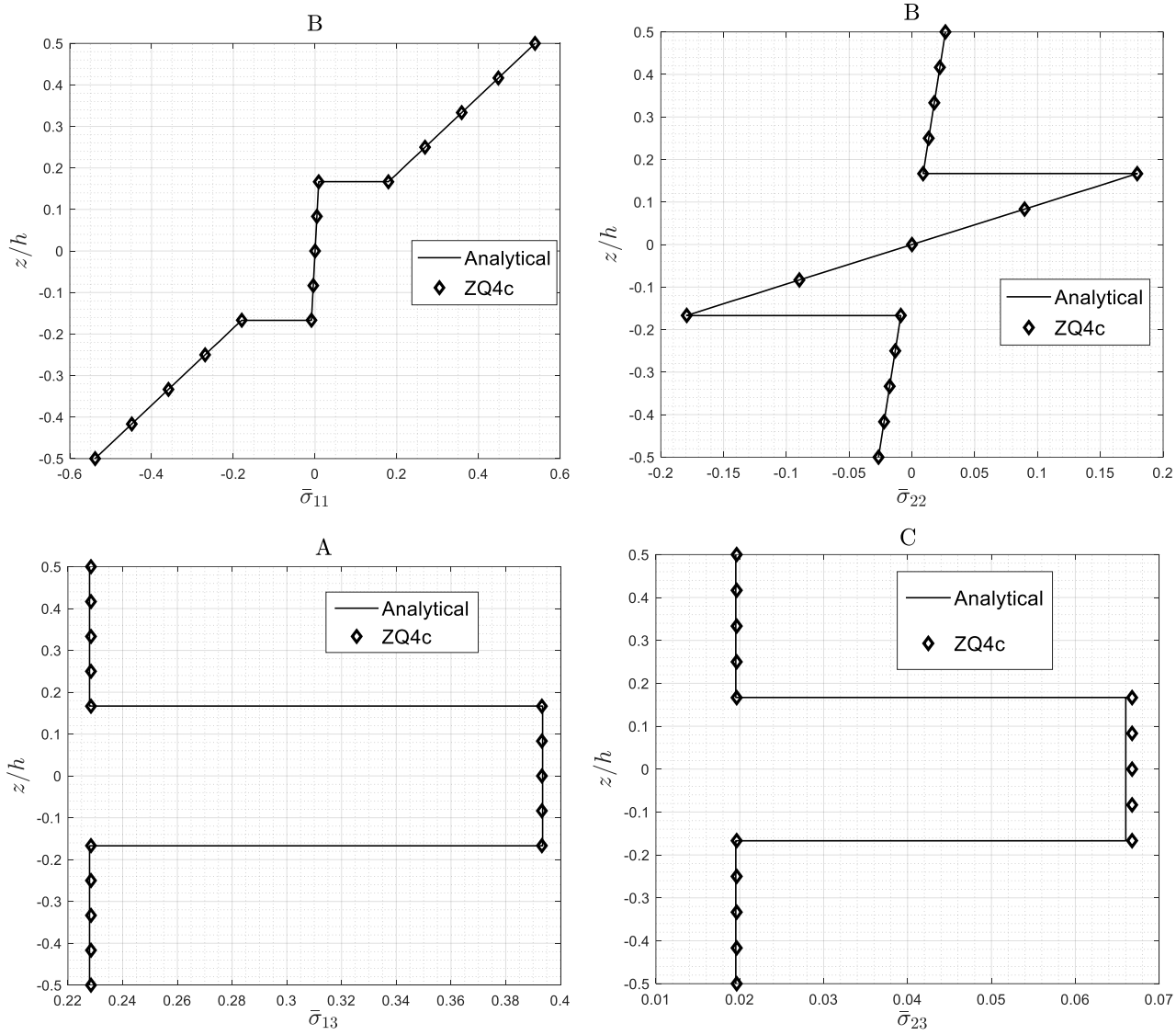

Figure 18 – Stress quantities evaluated in points A, B and C (see Figure 14) for thin (*a/h=10*^{6}) cross-ply (L1) simply supported square plate under bi-sinusoidal load.

The ZQ4c element is very accurate to predict the distributions for strains and stresses. Exceptionally good results have been obtained in thick regime when the transverse shear contribute is more pronounced. Furthermore, in thin regime, the distributions for transverse shear strains and stresses are very close with the analytical ones. Finer mesh patterns could improve the solution for the transverse shear strains and stresses in thin regime.

4.8 Bending moment and shear force distributions

To further assess the performance of ZQ4c, the bending moment and the transverse shear force distributions along the midline of the plate are compared with the corresponding analytic solutions. Two square plates (L1) are considered: a simply supported plate with the bi-sinusoidal load, and a cantilevered plate subjected to a uniform constant edge load $\bar{F}_{13}$. The plate models use the 17x17 element discretization: (i) a thick plate (*a/h=6*; *a/b=1*); (ii) a very thin plate (*a/h=10*^{6} ;

a/b=1). The analytic solutions have been obtained using the Ritz method [26] with 10 orthogonal functions in x_1 direction and 8 orthogonal functions in x_2 direction. The shear force and bending moment computed using the finite element correspond to the centroid of each element on the midline of the plate. The shear force and bending moment are normalized as follows,

a) bi-sinusoidal load condition:

$$\bar{T}_1 = \frac{T_1}{\bar{q}_0 a}; \qquad \bar{M}_{11} = \frac{M_{11}}{\bar{q}_0 a^2}$$

b) uniform constant edge load condition:

$$\bar{T}_1 = \frac{T_1}{\bar{F}_{13}}; \qquad \bar{M}_{11} = \frac{M_{11}}{\bar{F}_{13} a}$$

It should be noted that the integration of the transverse shear stresses as defined in the previous Section produces the following expressions for the element transverse shear force resultants (for symmetrical lamination):

$$\begin{aligned} T_1^{(e)} &= \phi_{(e)}^2 A_{t_{44}} \left[\mathbf{N}_{L,\xi} \mathbf{q}_w^{(e)} + \left(\mathbf{S}_{\theta_1,\xi} + \mathbf{N}_L \right) \mathbf{q}_{\theta_1}^{(e)} + \mathbf{S}_{\theta_2,\xi} \mathbf{q}_{\theta_2}^{(e)} + \mathbf{S}_{\psi_1,\xi} \mathbf{q}_{\psi_1}^{(e)} + \mathbf{S}_{\psi_2,\xi} \mathbf{q}_{\psi_2}^{(e)} \right] + \phi_{(e)}^2 B_{t_{44}}^{\psi} \mathbf{N}_L \mathbf{q}_{\psi_1}^{(e)} \\ T_2^{(e)} &= \phi_{(e)}^2 A_{t_{55}} \left[\mathbf{N}_{L,\eta} \mathbf{q}_w^{(e)} + \mathbf{S}_{\theta_1,\eta} \mathbf{q}_{\theta_1}^{(e)} + \left(\mathbf{S}_{\theta_2,\eta} + \mathbf{N}_L \right) \mathbf{q}_{\theta_2}^{(e)} + \mathbf{S}_{\psi_1,\eta} \mathbf{q}_{\psi_1}^{(e)} + \mathbf{S}_{\psi_2,\eta} \mathbf{q}_{\psi_2}^{(e)} \right] + \phi_{(e)}^2 B_{t_{55}}^{\psi} \mathbf{N}_L \mathbf{q}_{\psi_2}^{(e)} \end{aligned} \tag{65}$$

Note that Eq. (65) is the same as Eq. (48).

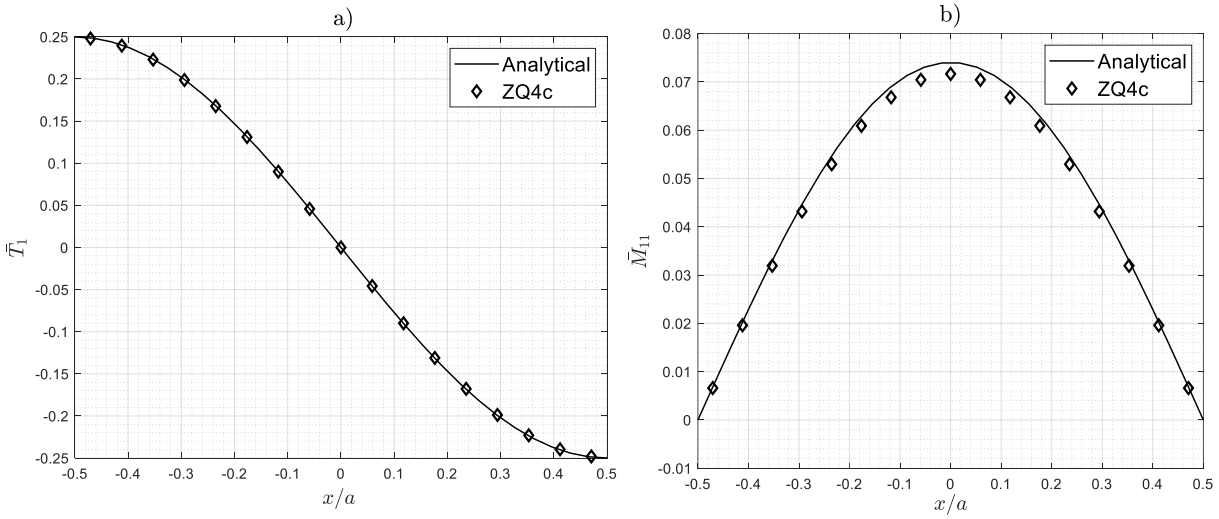

Figure 19 – Simply supported cross-ply (L1) square plate under bi-sinusoidal transverse pressure. Transverse shear force (a) and bending moment (b) distribution for span-to-thickness ratio (*a/h=6*).

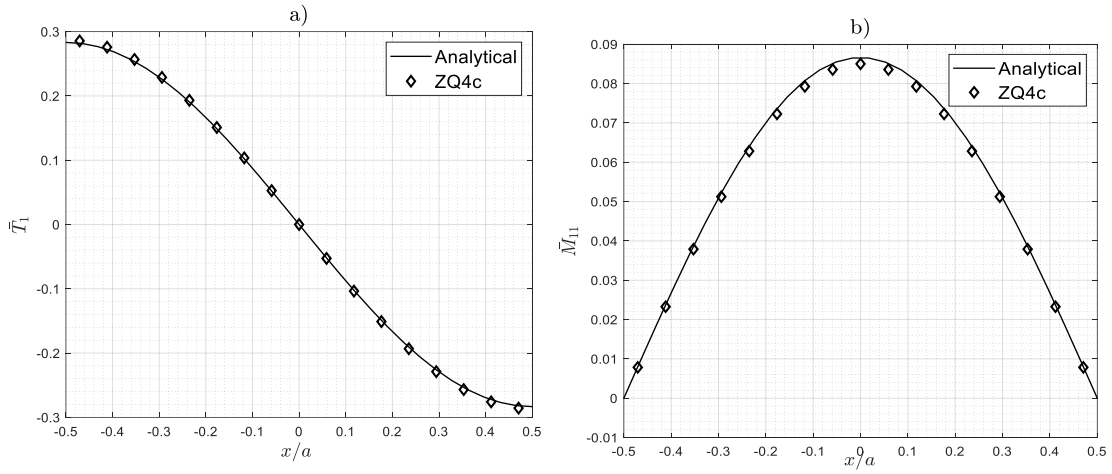

Figure 20 – Simply supported cross-ply (L1) square plate under bi-sinusoidal transverse pressure. Transverse shear force (a) and bending moment (b) distribution for span-to-thickness ratio ($a/h=10^6$).

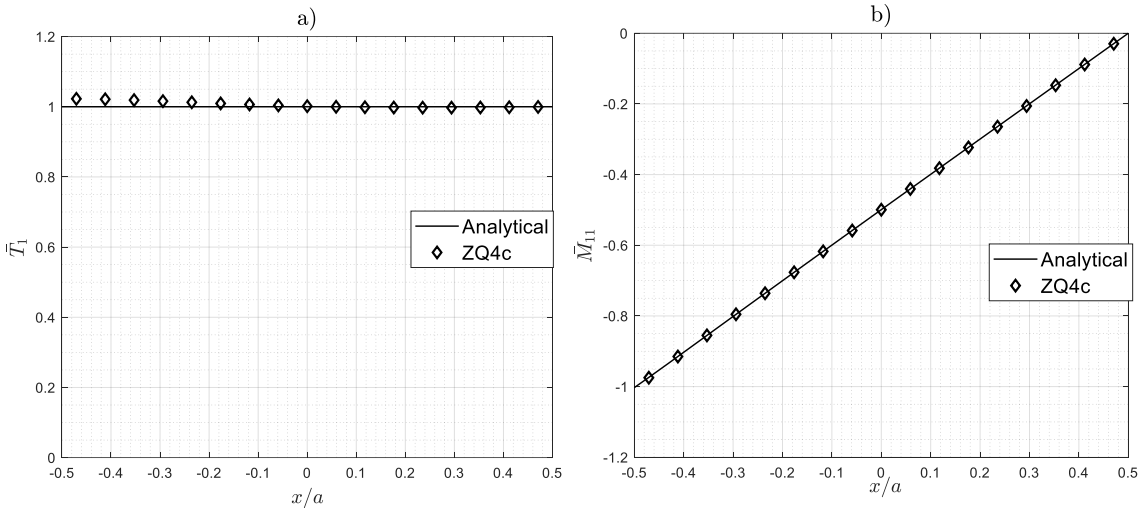

Figure 21 – Cantilever cross-ply (L1) square plate under constant edge transverse pressure. Transverse shear force (a) and bending moment (b) distribution for span-to-thickness ratio ($a/h=6$).

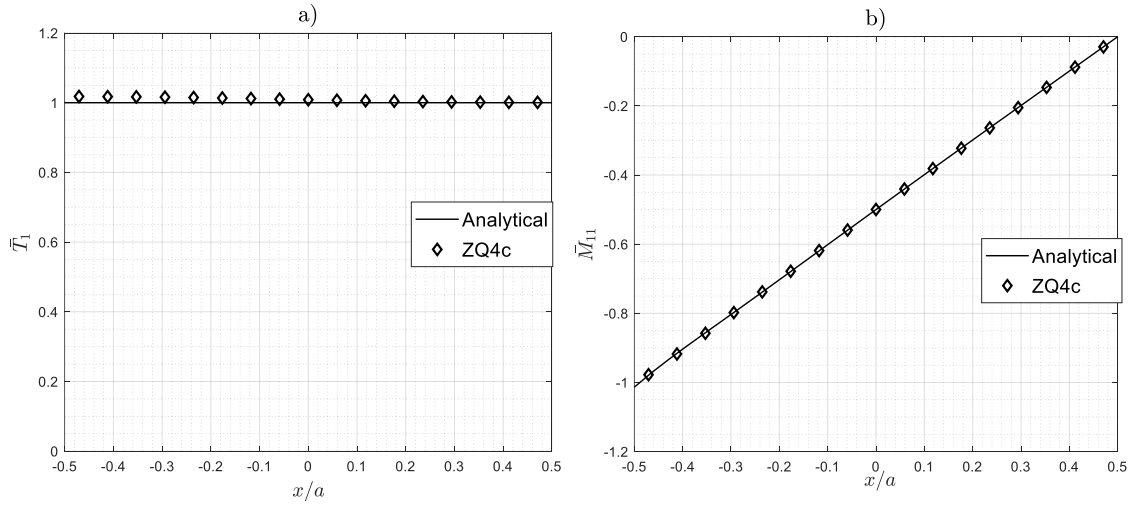

Figure 22 – Cantilever cross-ply (L1) square plate under constant edge transverse pressure. Transverse shear force (a) and bending moment (b) distribution for span-to-thickness ratio ($a/h=10^6$).

Figures 19-22 clearly demonstrate the high accuracy of ZQ4c predictions of transverse shear force and bending moment distributions for various span-to-thickness ratios, boundary conditions, and load cases.

5. Concluding remarks

The development of a robust, locking-free, four-node quadrilateral plate element for laminated composite and sandwich plates based on Refined Zigzag Theory has been presented. Initially, four- and eight-node isoparametric elements were examined. As expected, these elements demonstrated the detrimental effects of transverse shear locking in relatively thin and extremely thin plates. Subsequently, with the aim of alleviating the shear locking effect, the constrained *anisoparametric interpolation* strategy was adopted to formulate a simple and efficient four-node element. In addition, the element was further enhanced using the Element Shear Correction (ESC) factor, which was derived by way of a strain energy matching method. The resulting element, labeled ZQ4c, is free of locking even for extremely thin plates.

The element formulation uses the full Gauss quadrature to integrate the element stiffness matrix, consistent mass matrix, and consistent load vector, thus avoiding the spurious zero-energy modes that commonly arise when reduced integration is used to integrate the transverse shear strain energy. The effect of ESC is such that the element stiffness matrix is well-conditioned over the entire range of span-to-thickness ratios.

The ZQ4c element has demonstrated fast and monotonic convergence for moderately thick and extremely thin plates without suffering from transverse shear locking, verified up to $a/h=10^6$. Owing to the intrinsic properties of RZT, the element is capable of predicting accurate distributions of strains and stresses across the laminate thickness. The element is somewhat sensitive to geometric distortions, however, remarkably accurate results were consistently obtained for the transverse displacements, transverse shear resultants, bending moments, and natural frequencies, for various boundary conditions and load cases.

Further enhancements of the presented element can be achieved by extending the formulation to shell analysis, invoking the mixed-field $RZT^{(m)}$ formulation (based on Reissner's Mixed Variational Theorem), and by including von Karman's geometrically nonlinear effects. Finally, the present element may be viewed as an excellent candidate for inclusion into general-purpose finite element codes.

Acknowledgement

The third author, Dr. Alexander Tessler, a Distinguished Research Associate at NASA Langley Research Center, Hampton, Virginia, has contributed to this research while serving as a visiting professor in the Department of Mechanical and Aerospace Engineering, Politecnico di Torino, Italy. The support of the University and the Department are greatly appreciated.

Appendix A: ZQ4c element shape functions

The *unconstrained* quadrilateral element is based on *anisoparametric* interpolations. The shape functions for the variables $(u_1, u_2, \theta_1, \theta_2, \psi_1, \psi_2)$ are bi-linear, whereas the deflection, w, is interpolated using the eight-node serendipity shape functions. See Figure A.1 for RZT- *unconstrained* quadrilateral element geometry and nodal configuration.

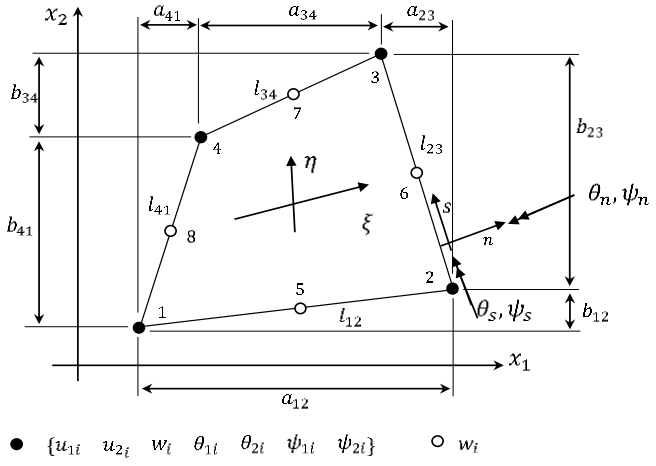

Figure A.1 – RZT-*unconstrained* quadrilateral plate element.

The shape functions are cast in the row-vector form as (refer to Eq. (34))

$$\mathbf{N}_L^{(e)} = \mathbf{N}_{u_1}^{(e)} = \mathbf{N}_{u_2}^{(e)} = \mathbf{N}_{\theta_1}^{(e)} = \mathbf{N}_{\theta_2}^{(e)} = \mathbf{N}_{\psi_1}^{(e)} = \mathbf{N}_{\psi_2}^{(e)} = \lfloor L_1 \quad L_2 \quad L_3 \quad L_4 \rfloor \tag{A.1}$$

$$\begin{gathered} \mathbf{N}_S^{(e)} = \mathbf{N}_w^{(e)} = \lfloor P_1 \quad P_2 \quad P_3 \quad P_4 \quad P_5 \quad P_6 \quad P_7 \quad P_8 \rfloor = \lfloor \mathbf{N}_C^{(e)} \quad \mathbf{N}_E^{(e)} \rfloor \\ \mathbf{N}_C^{(e)} = \lfloor P_1 \quad P_2 \quad P_3 \quad P_4 \rfloor; \qquad \mathbf{N}_E^{(e)} = \lfloor P_5 \quad P_6 \quad P_7 \quad P_8 \rfloor \end{gathered} \tag{A.2}$$

where the bi-linear Lagrange and eight-node serendipity shape functions are given, respectively, as

$$L_i(\xi,\eta) = \frac{1}{4}\left(1+\xi^{(i)}\xi\right)\left(1+\eta^{(i)}\eta\right) \ (i=1\div 4) \tag{A.3}$$

$$\begin{aligned} P_i\ (\xi,\eta) = {} & \frac{1}{4}\Big[(1+\xi^{(i)}\xi)(1+\eta^{(i)}\eta) - (1-\xi^2)(1+\eta^{(i)}\eta) - (1-\eta^2)(1+\xi^{(i)}\xi)\Big]\xi^{(i)2}\eta^{(i)2} + \\ & + \frac{1}{2}\Big[(1-\xi^2)(1+\eta^{(i)}\eta)\left(1-\xi^{(i)2}\right)\eta^{(i)2} + (1-\eta^2)(1+\xi^{(i)}\xi)\left(1-\eta^{(i)2}\right)\xi^{(i)2}\Big] \ (i=1\div 8) \end{aligned} \tag{A.4}$$

To achieve a four-node element configuration, a one-dimensional edge-constraint strategy is adopted, following the original ideas of Tessler and Dong [49] and Tessler and Hughes [50,51]. For RZT elements, a viable edge-constraint

strategy is to insist that the transverse shear strain measure, which involves both the bending rotation and zigzag amplitude variables,

$$\eta_{sz} = w_{,s} + \theta_n - \psi_n \tag{A.5}$$

be constant along the element edge, with s denoting the local edge coordinate; and where θ_n, ψ_n are the normal components of the edge bending rotation and zigzag amplitude, respectively (see Figure A.2). The key step in computing Eq. (A.5) is that the deflection w is first evaluated along the element edge and then differentiated with respect to s.

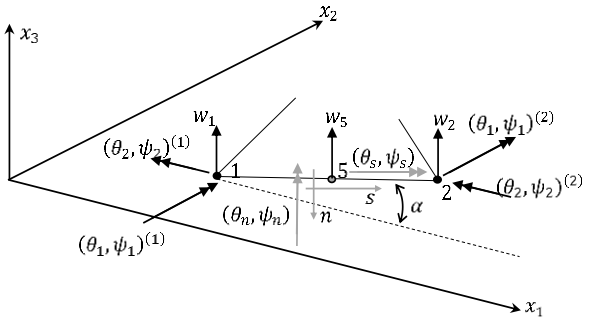

Figure A.2 - Nodal dof's (transverse deflection, bending rotations and zigzag amplitudes) and edge co-ordinate, s.

The constant edge-constraint condition can be expressed as

$$\eta_{sz,s} = 0 \tag{A.6}$$

The above constraint equation is preferred over a similar requirement on the *effective* transverse shear strain, previously examined in [40–42]. This is because if two adjacent elements with different transverse shear stiffness properties meet at a common edge, two incompatible deflection fields would have resulted along the common edge. The bending rotations and zigzag amplitude functions in Eq. (A.5) can be computed using appropriate orthogonal transformations, as

$$\theta_n = \theta_1 \cos\alpha + \theta_2 \sin\alpha; \qquad \psi_n = \psi_1 \cos\alpha + \psi_2 \sin\alpha \tag{A.7}$$

where α is the angle between the s and x_1 axes.

Substituting Eq. (A.7) in Eq. (A.5) and applying Eq. (A.6) results in

$$\eta_{sz,s} = w_{,ss} + \theta_{1,s}\cos\alpha + \theta_{2,s}\sin\alpha - \psi_{1,s}\cos\alpha - \psi_{2,s}\sin\alpha = 0 \tag{A.8}$$

Enforcing the above constraint condition along each element edge, the mid-edge deflection dof's are condensed out, resulting in the coupled form for the deflection variable, which is given in terms of the vertex nodal dof's of the deflection, bending rotations and zigzag amplitudes, as

$$w^{(e)} = \lfloor \mathbf{N}_L \quad \mathbf{S}_{\theta 1} \quad \mathbf{S}_{\theta 2} \quad \mathbf{S}_{\psi 1} \quad \mathbf{S}_{\psi 2} \rfloor \lfloor \mathbf{q}_w \quad \mathbf{q}_{\theta_1} \quad \mathbf{q}_{\theta_2} \quad \mathbf{q}_{\psi_1} \quad \mathbf{q}_{\psi_2} \rfloor^{(e)T} \tag{A.9}$$

where

$$\begin{aligned}\mathbf{S}_{\theta 1} &= -\mathbf{S}_{\psi 1} = \frac{1}{8}\begin{bmatrix} -a_{12}^{(e)}P_5 - a_{41}^{(e)}P_8 & a_{12}^{(e)}P_5 - a_{23}^{(e)}P_6 & a_{23}^{(e)}P_6 + a_{34}^{(e)}P_7 & -a_{34}^{(e)}P_7 + a_{41}^{(e)}P_8 \end{bmatrix} \\ \mathbf{S}_{\theta 2} &= -\mathbf{S}_{\psi 2} = \frac{1}{8}\begin{bmatrix} -b_{12}^{(e)}P_5 - b_{41}^{(e)}P_8 & b_{12}^{(e)}P_5 - b_{23}^{(e)}P_6 & b_{23}^{(e)}P_6 + b_{34}^{(e)}P_7 & -b_{34}^{(e)}P_7 + b_{41}^{(e)}P_8 \end{bmatrix}\end{aligned} \tag{A.10}$$

are the new shape functions given in terms of the edge projections defined as (see Figure A.1)

$$\begin{aligned} a_{12}^{(e)} &= x_1^{(2)} - x_1^{(1)}; \quad a_{23}^{(e)} = x_1^{(3)} - x_1^{(2)}; \quad a_{34}^{(e)} = x_1^{(3)} - x_1^{(4)}; \quad a_{41}^{(e)} = x_1^{(4)} - x_1^{(1)}; \\ b_{12}^{(e)} &= x_2^{(2)} - x_2^{(1)}; \quad b_{23}^{(e)} = x_2^{(3)} - x_2^{(2)}; \quad b_{34}^{(e)} = x_2^{(3)} - x_2^{(4)}; \quad b_{41}^{(e)} = x_2^{(4)} - x_2^{(1)}. \end{aligned} \tag{A.11}$$

Note that the shape functions in Eq. (A.10) are the same as those derived by Tessler and Hughes [50] for a Mindlin-type four-node quadrilateral element called MIN4.

References

[1] Abrate S, Di Sciuva M. Equivalent single layer theories for composite and sandwich structures: A review. Composite Structures 2017;179:482–94. https://doi.org/10.1016/j.compstruct.2017.07.090.

[2] Abrate S, Di Sciuva M. Multilayer Models for Composite and Sandwich Structures. In: Beaumont PWR, Zweben CH, editors. Comprehensive Composite Materials II, Elsevier; 2018, p. 399–425. https://doi.org/10.1016/B978-0-12-803581-8.09885-4.

[3] Madabhusi-Raman P, Davalos JF. Static shear correction factor for laminated rectangular beams. Composites Part B: Engineering 1996;27:285–93. https://doi.org/10.1016/1359-8368(95)00014-3.

[4] Ferreira AJM. A formulation of the multiquadric radial basis function method for the analysis of laminated composite plates. Composite Structures 2003;59:385–92. https://doi.org/10.1016/S0263-8223(02)00239-8.

[5] Reddy JN. Mechanics of Laminated Composite Plates and Shells : Theory and Analysis, Second Edition. CRC Press; 2003. https://doi.org/10.1201/b12409.

[6] Khoa NN, Thinh TI. Finite element analysis of laminated composite plates using high order shear deformation theory. Vietnam Journal of Mechanics 2007;29:47–57. https://doi.org/10.15625/0866-7136/29/1/5590.

[7] Lee SJ, Kim HR. FE analysis of laminated composite plates using a higher order shear deformation theory with assumed strains. Latin American Journal of Solids and Structures 2013;10:523–47. https://doi.org/10.1590/S1679-78252013000300005.

[8] Liew KM, Pan ZZ, Zhang LW. An overview of layerwise theories for composite laminates and structures: Development, numerical implementation and application. Composite Structures 2019;216:240–59. https://doi.org/10.1016/j.compstruct.2019.02.074.

[9] Di Sciuva M. A refinement of the transverse shear deformation theory for multilayered orthotropic plates. Proc. of AIDAA VII National Conference, vol. II, 1983, p. 83–95.

[10] Di Sciuva M. Bending, vibration and buckling of simply supported thick multilayered orthotropic plates: An evaluation of a new displacement model. Journal of Sound and Vibration 1986;105:425–42. https://doi.org/10.1016/0022-460X(86)90169-0.

[11] Di Sciuva M. An Improved Shear-Deformation Theory for Moderately Thick Multilayered Anisotropic Shells and Plates. J Appl Mech 1987;54:589–96. https://doi.org/10.1115/1.3173074.

[12] Di Sciuva M. Multilayered anisotropic plate models with continuous interlaminar stresses. Composite Structures 1992;22:149–67. https://doi.org/10.1016/0263-8223(92)90003-U.

[13] Di Sciuva M. A general quadrilateral multilayered plate element with continuous interlaminar stresses. Computers & Structures 1993;47:91–105. https://doi.org/10.1016/0045-7949(93)90282-I.

[14] Murakami H. Laminated Composite Plate Theory With Improved In-Plane Responses. J Appl Mech 1986;53:661–6. https://doi.org/10.1115/1.3171828.

[15] Icardi U. A three-dimensional zig-zag theory for analysis of thick laminated beams. Composite Structures 2001;52:123–35. https://doi.org/10.1016/S0263-8223(00)00189-6.

[16] Icardi U. Higher-order zig-zag model for analysis of thick composite beams with inclusion of transverse normal stress and sublaminates approximations. Composites Part B: Engineering 2001;32:343–54. https://doi.org/10.1016/S1359-8368(01)00016-6.

[17] Averill RC. Static and dynamic response of moderately thick laminated beams with damage. Composites Engineering 1994;4:381–95. https://doi.org/10.1016/S0961-9526(09)80013-0.

[18] Averill RC, Yip YC. Development of simple, robust finite elements based on refined theories for thick laminated beams. Computers & Structures 1996;59:529–46. https://doi.org/10.1016/0045-7949(95)00269-3.

[19] Tessler A, Di Sciuva M, Gherlone M. Refinement of Timoshenko Beam Theory for Composite and Sandwich Beams using Zigzag Kinematics. NASA/TP-2007-215086 2007:1–45.

[20] Tessler A, Di Sciuva M, Gherlone M. Refined Zigzag Theory for Laminated Composite and Sandwich Plates. NASA/TP-2009-215561 2009:1–53.

[21] Versino D, Gherlone M, Di Sciuva M. Four-node shell element for doubly curved multilayered composites based on the Refined Zigzag Theory. Composite Structures 2014;118:392–402. https://doi.org/10.1016/j.compstruct.2014.08.018.

[22] Tessler A, Di Sciuva M, Gherlone M. A homogeneous limit methodology and refinements of computationally efficient zigzag theory for homogeneous, laminated composite, and sandwich plates. Numerical Methods for Partial Differential Equations 2011;27:208–29. https://doi.org/10.1002/num.20646.

[23] Gherlone M. On the Use of Zigzag Functions in Equivalent Single Layer Theories for Laminated Composite and Sandwich Beams: A Comparative Study and Some Observations on External Weak Layers. J Appl Mech 2013;80:061004-061004–19. https://doi.org/10.1115/1.4023690.

[24] Iurlaro L, Gherlone M, Di Sciuva M, Tessler A. Assessment of the Refined Zigzag Theory for bending, vibration, and buckling of sandwich plates: a comparative study of different theories. Composite Structures 2013;106:777–92. https://doi.org/10.1016/j.compstruct.2013.07.019.

[25] Iurlaro L, Gherlone M, Di Sciuva M. Bending and free vibration analysis of functionally graded sandwich plates using the Refined Zigzag Theory. Jnl of Sandwich Structures & Materials 2014;16:669–99. https://doi.org/10.1177/1099636214548618.

[26] Di Sciuva M, Sorrenti M. Bending and free vibration analysis of functionally graded sandwich plates: An assessment of the Refined Zigzag Theory. Journal of Sandwich Structures & Materials 2019:1–43. https://doi.org/10.1177/1099636219843970.

[27] Di Sciuva M, Sorrenti M. Bending, free vibration and buckling of functionally graded carbon nanotube-reinforced sandwich plates, using the extended Refined Zigzag Theory. Composite Structures 2019:111324. https://doi.org/10.1016/j.compstruct.2019.111324.

[28] Groh RMJ, Weaver PM. On displacement-based and mixed-variational equivalent single layer theories for modelling highly heterogeneous laminated beams. International Journal of Solids and Structures 2015;59:147–70. https://doi.org/10.1016/j.ijsolstr.2015.01.020.

[29] Groh RM, Weaver PM, Tessler A. Application of the Refined Zigzag Theory to the Modeling of Delaminations in Laminated Composites. NASA/TM-2015-218808 2015:1–22.

[30] Dorduncu M. Stress analysis of laminated composite beams using refined zigzag theory and peridynamic differential operator. Composite Structures 2019;218:193–203. https://doi.org/10.1016/j.compstruct.2019.03.035.

[31] Tessler A. Refined zigzag theory for homogeneous, laminated composite, and sandwich beams derived from Reissner's mixed variational principle. Meccanica 2015;50:2621–48. https://doi.org/10.1007/s11012-015-0222-0.

[32] Groh RMJ, Tessler A. Computationally efficient beam elements for accurate stresses in sandwich laminates and laminated composites with delaminations. Computer Methods in Applied Mechanics and Engineering 2017;320:369–95. https://doi.org/10.1016/j.cma.2017.03.035.

[33] Iurlaro L, Gherlone M, Di Sciuva M, Tessler A. Refined Zigzag Theory for laminated composite and sandwich plates derived from Reissner's Mixed Variational Theorem. Composite Structures 2015;133:809–17. https://doi.org/10.1016/j.compstruct.2015.08.004.

[34] Gherlone M, Tessler A, Di Sciuva M. C^0 beam elements based on the Refined Zigzag Theory for multilayered composite and sandwich laminates. Composite Structures 2011;93:2882–94. https://doi.org/10.1016/j.compstruct.2011.05.015.

[35] Oñate E, Eijo A, Oller S. Simple and accurate two-noded beam element for composite laminated beams using a refined zigzag theory. Computer Methods in Applied Mechanics and Engineering 2012;213–216:362–82. https://doi.org/10.1016/j.cma.2011.11.023.

[36] Eijo A, Oñate E, Oller S. A numerical model of delamination in composite laminated beams using the LRZ beam element based on the refined zigzag theory. Composite Structures 2013;104:270–80. https://doi.org/10.1016/j.compstruct.2013.04.035.

[37] Di Sciuva M, Gherlone M, Iurlaro L, Tessler A. A class of higher-order C^0 composite and sandwich beam elements based on the Refined Zigzag Theory. Composite Structures 2015;132:784–803. https://doi.org/10.1016/j.compstruct.2015.06.071.

[38] Eijo A, Oñate E, Oller S. A four-noded quadrilateral element for composite laminated plates/shells using the refined zigzag theory. International Journal for Numerical Methods in Engineering 2013;95:631–60. https://doi.org/10.1002/nme.4503.

[39] Eijo A, Oñate E, Oller S. Delamination in laminated plates using the 4-noded quadrilateral QLRZ plate element based on the refined zigzag theory. Composite Structures 2014;108:456–71. https://doi.org/10.1016/j.compstruct.2013.09.052.

[40] Versino D, Gherlone M, Mattone MC, Di Sciuva M, Tessler A. C^0 triangular elements based on the Refined Zigzag Theory for multilayered composite and sandwich plates 2013;44B:218–30. https://doi.org/10.1016/j.compositesb.2012.05.026.

[41] Di Sciuva M, Sorrenti M. A Family of C^0 Quadrilateral Plate Elements Based on the Refined Zigzag Theory for the Analysis of Thin and Thick Laminated Composite and Sandwich Plates. Journal of Composites Science 2019;3:100. https://doi.org/10.3390/jcs3040100.

[42] Gherlone M. Tria and quad plate finite elements based on RZT(m) for the analysis of multilayered sandwich structures. Composite Structures 2019;220:510–20. https://doi.org/10.1016/j.compstruct.2019.04.032.

[43] Gherlone M, Versino D, Zarra V. Multilayered triangular and quadrilateral flat shell elements based on the Refined Zigzag Theory. Composite Structures 2019:111629. https://doi.org/10.1016/j.compstruct.2019.111629.

[44] Zienkiewicz OC, Taylor RL, Too JM. Reduced integration technique in general analysis of plates and shells. International Journal for Numerical Methods in Engineering 1971;3:275–90. https://doi.org/10.1002/nme.1620030211.

[45] Belytschko T, Jame Shau-Jen Ong, Wing Kam Liu. A consistent control of spurious singular modes in the 9-node Lagrange element for the Laplace and Mindlin plate equations. Computer Methods in Applied Mechanics and Engineering 1984;44:269–95. https://doi.org/10.1016/0045-7825(84)90133-6.

[46] Belytschko T, Leviathan I. Physical stabilization of the 4-node shell element with one point quadrature. Computer Methods in Applied Mechanics and Engineering 1994;113:321–50. https://doi.org/10.1016/0045-7825(94)90052-3.

[47] Reese S, Wriggers P. A stabilization technique to avoid hourglassing in finite elasticity. International Journal for Numerical Methods in Engineering 2000;48:79–109. https://doi.org/10.1002/(SICI)1097-0207(20000510)48:1<79::AID-NME869>3.0.CO;2-D.

[48] Cardoso RPR, Yoon JW. One point quadrature shell element with through-thickness stretch. Computer Methods in Applied Mechanics and Engineering 2005;194:1161–99. https://doi.org/10.1016/j.cma.2004.06.017.

[49] Tessler A, Dong SB. On a hierarchy of conforming timoshenko beam elements. Computers & Structures 1981;14:335–44. https://doi.org/10.1016/0045-7949(81)90017-1.

[50] Tessler A, Hughes TJR. An improved treatment of transverse shear in the Mindlin-type four-node quadrilateral element. Computer Methods in Applied Mechanics and Engineering 1983;39:311–35. https://doi.org/10.1016/0045-7825(83)90096-8.

[51] Tessler A, Hughes TJR. A three-node Mindlin plate element with improved transverse shear. Computer Methods in Applied Mechanics and Engineering 1985;50:71–101. https://doi.org/10.1016/0045-7825(85)90114-8.

[52] Tessler A, Spiridigliozzi L. Curved beam elements with penalty relaxation. International Journal for Numerical Methods in Engineering 1986;23:2245–62. https://doi.org/10.1002/nme.1620231207.

[53] Tessler A. A C^0-anisoparametric three-node shallow shell element. Computer Methods in Applied Mechanics and Engineering 1990;78:89–103. https://doi.org/10.1016/0045-7825(90)90154-E.

[54] Liu J, Riggs HR, Tessler A. A four-node, shear-deformable shell element developed via explicit Kirchhoff constraints. International Journal for Numerical Methods in Engineering 2000;49:1065–86. https://doi.org/10.1002/1097-0207(20001120)49:8<1065::AID-NME992>3.0.CO;2-5.

[55] Tessler A, Di Sciuva M, Gherlone M. A consistent refinement of first-order shear-deformation theory for laminated composite and sandwich plates using improved zigzag kinematics. Journal of Mechanics of Materials and Structures 2010;5:341–67. https://doi.org/10.2140/jomms.2010.5.341.

[56] Pagano NJ. Exact Solutions for Rectangular Bidirectional Composites and Sandwich Plates. Journal of Composite Materials 1970;4:20–34. https://doi.org/10.1177/002199837000400102.

[57] Barut A, Madenci E, Tessler A. A Refined Zigzag Theory for Laminated Composite and Sandwich Plates Incorporating Thickness Stretch Deformation. 53rd AIAA/ASME/ASCE/AHS/ASC Structures, Structural Dynamics and Materials Conference, American Institute of Aeronautics and Astronautics; 2012. https://doi.org/doi.org/10.2514/6.2012-1705.

[58] Iurlaro L, Gherlone M, Di Sciuva M. The (3,2)-Mixed Refined Zigzag Theory for generally laminated beams: Theoretical development and C^0 finite element formulation. International Journal of Solids and Structures 2015;73–74:1–19. https://doi.org/10.1016/j.ijsolstr.2015.07.028.